Effect of Velocity Gradient and Floc Characteristics on Membrane Fouling

By

HIRA AMJAD

Institute of Environmental Sciences & Engineering (IESE)

School of Civil & Environmental Engineering (SCEE)

National University of Sciences & Technology (NUST)

2016

Effect of Velocity Gradient and Floc Characteristics on Membrane Fouling

HIRA AMJAD   2009-NUST-TfrPhD-Env-96

This work is submitted as a PhD thesis in partial fulfillment of the requirement for the degree of

(PhD in Environmental Engineering)

Supervisor: Dr. Sher Jamal Khan

**Institute of Environmental Sciences & Engineering (IESE)
School of Civil & Environmental Engineering (SCEE)
National University of Sciences & Technology (NUST),
Islamabad, Pakistan**

2016

Certificate

Certified that the contents and form of thesis entitled "Effect of Velocity Gradient and Floc Characteristics on Membrane Fouling" submitted by Ms. Hira Amjad have been found satisfactory for the requirement of the degree.

Supervisor**: _____**
Dr. Zahiruddin Khan
Associate Professor (IESE-SCEE, NUST)

GEC Members

Dr. Ishtiaq A. Qazi
Professor (IESE, SCEE, NUST)

Co-supervisor (Internal)_____
Dr. Sher Jamal
Associate Professor (IESE, SCEE, NUST)

Co-supervisor (External)_____
Dr. Volodymyr. V. Tarabara
Associate Professor
Department of Civil and Environmental Engineering, Michigan State University, USA

Dedicated

to

my beloved family

&

Me

TABLE OF CONTENTS

LIST OF TABLES

LIST OF FIGURES

LIST OF ABBREVIATIONS

AD	Alum dose
T	Temperature
HA	Humic acid
D_fFloc (M)	D_f of flocs measured by Malvern Mastersizer
D_fFloc (B)	D_f of flocs measured by box counting
NTU	Nephelometric Turbidity Unit
LT	Low turbidity water

LIST OF SYMBOLS

G	Velocity gradient (sec^{-1})
T	Residence time (Coagulation and flocculation), Elapsed time (filtration)
UC	Uniformity coefficient
ξ	Zeta potential (mV)
T	Absolute temperature (^{o}K)
μ	Dynamic viscosity of the fluid ($N\text{-}s/m^2$)
HLR	Hydraulic loading rate, defined as flow rate divided by filtration cross-sectional area (mm/sec)
α	Filter attachment coefficient (dimensionless)
λ	Filter coefficient (cm^{-1})
η	Filter transport coefficient (dimensionless)
FI	Flocculation index

EFFECT OF VELOCITY GRADIENT AND FLOC CHARACTERISTICS ON MEMBRANE FOULING

ABSTRACT

Effects of coagulation-flocculation pretreatment and settling on the flux performance of ultrafiltration membranes were studied and results were interpreted in terms of structural characteristics of flocs and membrane cakes formed by the flocs. To find out the fractal dimension of membrane cake experimentally, a new non-invasive method was proposed and tested by applying to experimental data of membrane filtration. In first phase (section A) of this study, two types of clay suspensions (medium and low turbidity) were used within a pH range of 5.5-7.5. Clay flocs were produced under low and high $\bar{G}t_{mix}$ conditions with an alum dose range of 3-6.5mg/L. In second phase (section B), humic acid flocs were produced under three $\bar{G}t_{mix}$ conditions (50,400, 17,820 and 1,890) within a pH range of 4.8 to 5.5 at an alum dose of 70 mg/L. Different coagulation-flocculation conditions produced flocs of different microstructures and ultimately membrane cakes of different permeabilities. Larger flocs with higher fractal dimension D_f, were produced by high $\bar{G}t_{mix}$ and conditions of medium and low $\bar{G}t_{mix}$ produced flocs of relatively low D_f. Experiments where the settling was provided to suspended clay and humic acid flocs, prior to ultrafiltration, led to the production of very dense membrane cakes with less porosity and high specific cake resistance (α_m). In experiments where the settling was not provided to suspended clay and humic acid flocs prior to ultrafiltration, the membrane cakes were

highly porous having lower specific cake resistance (α_m). As a result, high $\bar{G}t_{mix}$-S experiments translated into highest specific cake resistance (α_m) and medium $\bar{G}t_{mix}$-N experiments translated into lowest specific cake resistance (α_m). Fractal dimension of the flocs produced using humic acid solution were well correlated with fractal dimension of membrane cakes of constituent flocs whereas, fractal dimensions of clay flocs were poorly correlated to fractal dimensions of membrane cakes.

INTRODUCTION

1.1 BACKGROUND

A recent trend in the development of water purification technologies is towards decreasing redundancy without compromising the robustness of the treatment. Novel technologies such as membrane filtration enable such efforts; for example, in conventional, direct and in-line filtration trains, ultra- and micro-membranes can replace sand.

Water filtration, was generally considered as a polishing, though vital, step in the conventional treatment system. With time and experience, it has become the most important barrier between human health and disease-causing microorganisms. The importance of the filtration step increases in the absence of sedimentation (as in direct filtration plants), and, even more so, in the absence of both flocculation and sedimentation (as in in-line filtration plants.)

Addition of coagulants and flocculation aids, i.e., alum, ferric chloride and/or other long chain polymers for the removal of charged colloidal matter from drinking water supply is the widely accepted phenomenon (AWWA, 1997). Colloidal particles when present in water exhibit the electrical charge and because of their similar charge they

repel each other and remain suspended in water for long time. This suspension ultimately counts as turbidity and is undesirable according to drinking water quality standards. In coagulation process various chemicals are added to the water to reduce the charge on these particles so that these particles can form aggregates which are easier to settle due to their high density and large size (Metcalf and Eddy, 2003). The pre-coagulation behind a membrane has two major benefits; it reduces the plant footprint compared to a standard clarification process (the use of membranes avoids the need for settling tanks), and it reduces the fouling of the membrane by individual colloids/molecules.

Particulate removal via microfiltration and ultrafiltration membranes depends upon many factors including floc properties (e.g., charge, size, shape and strength), operational parameters of membrane filtration (e.g., permeate and crossflow flux) and physico-chemical properties of the membrane (e.g., pore size, roughness, hydrophilicity). Particles destabilized during coagulation get transported to the membrane and can get attached to its surface or to an already attached particle through electrostatic and van der Waal's forces as well as due to non-DLVO interactions. In most cases, weak, fragile flocs tend to accumulate on the membrane surface in the form of cake layer leading to membrane fouling and higher requirements of trans-membrane pressure differentials to enable the same product water flux. This translates into more frequent backwashing of membranes and, ultimately, shorter membrane life. Flocs penetrability can be enhanced by tailoring the coagulation process to produce

stronger, more shear resistant pin-head sized flocs. Major factors controlling floc characteristics are the type and dosage of coagulant used and the mixing conditions.

Destabilized colloidal matter agglomerate into larger particles called flocs. The rate of aggregation and break-up during coagulation/flocculation process determines the floc size distribution (Rattanakawin and Hogg, 2001; Jarvis et al., 2005; Bouyeret al., 2005). Physicochemical and hydrodynamic conditions are particularly important factors in floc size distribution. As the value of velocity gradient (G) fluctuates, the changes occur in floc structure. The fractal dimension of flocs had been, measured and analyzed by experimental, numerical simulation and theoretical methods. Fractal aggregates contain various active sites on their surface according to diffusion-limited aggregation (DLA) and other theoretical analysis (Witten and Sander, 1981; Terao and Nakayama, 1998; Tanaka and Araki, 2000). Fractal characteristics of flocs mean that they are self similar and scale invariant (Jiang and Logan, 1991; Johnsonet al., 1996; Gregory, 1997; Chakrabortiet al., 2000). For characterization of the floc structure, floc strength, floc fractal dimension and detection of scale variance are significant factors. "Light scattering image analysis" and "settling" are the most commonly used methods for the recognition of fractal dimensions (Wu et at., 2002; Koen and Willy, 1997; Chakrabortiet al., 2003; Tang, 2002). The aggregates having high fractal dimensions are generally compact and small in size, whereas, aggregates having low fractal dimensions are loose, branched and fragile in nature.

Floc strength is one of the basic characteristic of flocs and it reflects the efficiency of solid-liquid separation in water treatment system. Flocs that are once formed during

coagulation process tend to break-up due to uneven shear distribution. So flocs must be strong enough to withstand the shear fluctuations in the flocculation basin for efficient removal of flocs from water. Small and loosely connected clusters of flocs reduce the removal efficiency of filter because of surface cake formation. Colloidal particles form bonds when they come close to each other and the strength of flocs formed depends on these bonds (Jiang and Logan, 1991; Tambo and Watanabe, 1978; Tambo and Hozumi, 1979; Johnsonet al., 1996; Bache et al., 1999).

Mixing is very important to homogeneously disperse the precipitating agents i.e., coagulants and coagulant aids in the water. It stimulates the process of rapid precipitation reactions leading to floc growth and settling of precipitates. For a typical mixing tank, the degree of mixing is dependent upon the amount of energy induced in terms of mixing, residence time and turbulence resulted from the shape of the mixing tank. Mixing can be of two types: flash or rapid mixing, and continuous mixing. Both types are widely used in coagulation/flocculation process. The purpose of rapid or flash mixing is to evenly disperse the coagulant throughout the body of liquid. While slow mixing play a significant role in formation of floc aggregates of the destabilized particles. The power applied per unit volume measured in terms of velocity gradient, can be used as a rough estimate of mixing effectiveness. The most commonly used equation for the determination of velocity gradient is (Metcalf and Eddy, 2003):

$$G = [P/\mu V]^{1/2}$$

(i)

Whereas, G is mean velocity gradient (s^{-1}); P is power input (W) or (ftlb/s); μ is dynamic viscosity (N s/m^2) or (lb s/ft^2) and V is tank volume (m^3) or (ft^3).

Membrane filtration is the technology which can fulfill the increasing demand of drinking water as it has the capacity to treat water from sources of a wide range (Byun, 2011). Although microfiltration is a very useful technique and has high treatment efficiencies, yet membrane technology is being explored by researchers everywhere for its application in water and wastewater treatment on large scale (Le-Clech et al., 2006; Zularisam et al., 2006; Meng et al., 2009; Huang et al., 2010;).

Coagulation prior to membrane filtration helps reducing colloidal pressure over membranes as well as enhances the membrane efficiency and prolongs its operational life. However, production of tough micro-flocs amenable to membrane filtration requires excellent control on factors affecting coagulation outcome.

The optimal design of the coagulation-membrane filtration process requires deeper understanding of underlying processes that can be used to formulate algorithms connecting feed water quality with operational parameters. By addressing existing knowledge gaps the proposed research project will contribute to the development of science-based treatment algorithms for use by practitioners in the water treatment field.

1.2 PROBLEM STATEMENT

Over the past two decades membrane filtration has been rapidly replacing conventional rapid rate filtration systems. Most studies on pre-treatment (coagulation) of water

before membrane treatment ignored any link between coagulation conditions and floc characteristics. While the effect of rapid mixing on alum floc has been studied by many researchers (Spicer and Pratsinis, 1996; Waite, 1999; Colomer et al., 2005; Xiao et al., 2010; Rojas et al., 2010;), the impacts of floc characteristics on the performance of downstream membrane filtration have not been clearly established. This study aimed at filling this knowledge gap. Specifically, the goal was to establish the links between 1) coagulation parameters, 2) floc properties, and 3) membrane performance, quantified in terms of turbidity removal and flux decline using MF and UF membranes.

a) **PURPOSE**

The purpose of this research was to advance the rational basis for the design and operation of the in-line filtration process with special emphasis on membrane filtration (MF/UF). The focus remained on relating the coagulation and membrane filtration process to floc characteristics, developed under certain coagulation conditions (i.e., G, t etc.) and the effect of these flocs on membrane performance.

1.3 OBJECTIVES

Whilst the main objective of this research was to determine how the coagulation process variables affect floc characteristics, and how the floc characteristics affect membrane fouling and flux rates. Specific objectives included:

    i.   To study the influence of variations in velocity gradient (G), on alum floc characteristics i.e., size, strength, shape and fractal dimension and effect of

floc characteristics on MF and UF membranes under a range of hydraulic loading rates.

ii. To elucidate dominant mechanisms of membrane fouling during ultra- and microfiltration of pre-coagulated water.

iii. To compare the effectiveness of treatment by polymeric ultra- and micro-filtration membranes of varying porosities.

1.4 SCOPE OF STUDY

Major variables involved in coagulation/flocculation and microfiltration processes include: raw water characteristics, coagulant type and dose, rate of rapid mix velocity gradient (G), detention time (T), initial permeate flux, crossflow rate, membrane hydrophilicity, and membrane pore size. Variation in some of the variables may have major impact on the effectiveness of the treatment process without substantially affecting the overall cost of operation while others may have only a minor, if any, effect. The proposed research was focused on the effect of "G" on floc properties and the efficiency of filtration by membranes of various pore sizes at the optimum coagulant dose. Such knowledge would help designing coagulation systems compatible with membrane properties and provision of larger quantities of water with prolonged membrane operations.

LITERATURE REVIEW

Contaminated drinking water requires appropriate treatment to remove these contaminants. Naturally, surface water (lakes, streams and rivers) are more subject to contamination than the ground water bodies and also surface water requires more treatment and filtration than the ground water. A diverse range of treatment technologies can be applied to decontaminate the drinking water. Treatment technologies are selected and applied using several determining factors including water source, type of contaminant, and cost. For the most effective treatment, a combination of technologies is used to insure that water is treated to required standards.

2.1 TURBIDITY IN NATURAL WATER

Natural waters have suspended particles and dissolved species of various origin, size, concentration, and surface chemistry. Some of them come from land-based sources i.e., silt and clay. Colloidal particles are usually the smallest particles with a size of one dimension less than 1 µm. Most suspended particles are larger though. Turbidity is one of the principal predictors of the performance of particle removal processes in water treatment systems. In the past, turbidity measurements were carried out to measure the aesthetic quality of treated water. USEPA lowered the turbidity limit for treated water to 1 NTU after the passage of the Safe Drinking Water Act in 1974. The explanation for that lower limit was that particles responsible for turbidity could

interfere with disinfection process in water treatment as they enmesh with and protect the microorganisms from chlorination. Turbidity can also be used to evaluate the performance of a granular medium filter (Letterman et al., 1999).

2.2 NATURAL ORGANIC MATTER IN NATURAL WATER

Presence of organic matter in source water is not desirable because it is a main cause of color in water, a reason for the formation of carcinogenic byproducts in a course of disinfection by chlorine (Siddiqui et al., 1997; Khan et al., 1998). Humic acids are a heterogeneous mixture of aromatic and aliphatic components and it's a basic natural organic matter (NOM) with three main functional groups: carboxylic acids (COOH), methoxy carbonyls (C=O) and phenolic alcohols (OH) (Dennett et al., 1995). A negative charge is found on humic substances when ionization of carboxyl groups occurs. According to Ghosh and Schnitzer (1980) and Cornet et al. (1986) the structural range of humic acid is from rigid sphero-colloidal to flexible linear. The compact form of humic acid molecules is found in a water sample where the concentration of humic acids is high, pH is low and an ample amount of neutral electrolytes are present. The structure is more linear when the water sample has less concentration of humic acid, pH is alkaline or neutral and the ionic strength is relatively low (Wang et al., 2010).

2.3 COAGULATION

Coagulation and sedimentation are common processes used to destabilize and remove suspended particles and some larger dissolved species from water and wastewater. The theory behind this process is to reduce the charge on the particles and to enhance the collision frequency so that the particles can aggregate into large flocs and settle down quickly. Larger particles tend to settle down quicker allowing for smaller hydraulic retention times (Serra et al., 1997). Using metal salts for coagulation is a widely accepted practice in water treatment. In this process microscopic particles can be grown in size by minimizing the repulsive potential of electrical double layers of colloids (Matilainen et al., 2010).

2.3.1 Velocity Gradient

Some of the previous studies indicated that larger shear rates lead to the smaller aggregate size under steady state conditions (Oles, 1992; Serra et al., 1997). All the work was conducted at $G \geq 25$ s^{-1} (Zhan et al., 2011). The aggregation and breakup of flocs under low shear rates (0.70 s^{-1} < G < 27.36 s^{-1}) were examined by Colomer et al. in 2005 and they observed an increase in floc size with increasing G values. Spicer and Pratsinis (1996) studied the influence of various impeller devices on the formation and break-up of flocs while using a broad range of G values (ranging from 4 s^{-1} to 102 s^{-1}). Moreover, Serra et al. in 2008 focused on particle size spectra as influenced by three different laboratory devices (paddle mixer, oscillating grid and coquette) while keeping the G values between 4 s^{-1} and 102 s^{-1}. Xiao et al. in 2010 showed that the

steady floc sizes of the particles in the suspension became smaller and more regular, when slow-mixing speed was increased. The studies conducted in the past had only focused on coagulation of particles and their characteristics. Except a study conducted by Rojas et al. in 2010 who investigated the various G values as their impact on membrane clogging for removal of natural organic matter (NOM). Flocs size and shape is largely dependent on the value of velocity gradient (G), as the velocity gradient varies different types of flocs are formed and effect the efficiency of water treatment process (Rojas et al., 2010).

To observe the impact of velocity gradient (G) on floc characteristics in a coagulation process a study was conducted by Xiao, et al. in 2011. Pre-hydrolyzed coagulants (polyaluminum chloride, denoted as PAC, and polyferric chloride, denoted as PFC) were used to study the effect of different velocity gradient values (G ranging from 4.4 s^{-1} to 28.3 s^{-1}) on the flocculation performance and floc properties from the low organic matter (OM) surface water. The results show that highest turbidity removal was achieved at G= 7.6 s^{-1} and 15.2 s^{-1} respectively for PFC and PAC (Zhan et al., 2011).

2.4 FLOCCULATION

The first step in the coagulation process is supposed to be a rapid initial growth of the particles. As the particles become fully destabilized, they eventually form small aggregates. When the aggregates enter into the flocculation phase they become larger and their structures are fragile that can easily broken-up by hydrodynamic forces. At the flocculation stage there is a smaller number of aggregates but they are larger in

size, and their further growth ceases. Ultimately a pseudo-steady state is established in the particle size distribution, where a balance is created between the aggregation and break-up, and the size spectra remain constant (Oles, 1992). Although the aggregate size increases in flocculation stage, the increasing shear rate decreases the aggregate growth rate (Serra et al., 1997).

2.4.1 Floc Structure

The important parameters for floc structure definition are its size, shape and density. These parameters can be changed with different flocculation conditions in peri- and ortho-kinetic flocculation. Floc filterability is highly dependent on these parameters (Cho et al., 2005).

2.4.2 Floc Formation and Breakage

Past studies indicate that flocs breakage and re-growth increases the residual turbidity in water. But the efficiency of coagulation and flocculation can be improved by flocs breakage and re-growth under certain conditions. The formation, breakage and re-growth of flocs were studied using alum and PACl as coagulants for water with kaolin clay and/or kaolin clay and humic acid. Full re-growth in kaolin water occurs under charge neutralization conditions. But under sweep flocculation, re-growth is very minor. Irrespective of previous studies this study shows that the residual turbidity was lower after breakage and re-growth than before the breakage and re-growth (Yu et al., 2009).

When pre-coagulated flocs are exposed to high shear rates, the flocs break-up and their newly formed surfaces may have positive, negative or neutral charge depending on the coagulation process applied for the formation and break-up of flocs (McCurdy et al., 2004). In coagulation process when the mechanism of charge neutrality dominates, some of the particles adsorb Al^{3+} and become positively charged. These positively charged particles now attach to negatively charged particles and increase in size. There are also a number of particles in water which do not combine with other particles, remain in water and contribute to residual turbidity. Generally, charge neutralization process produces more compact flocs (Tan et al., 2007) surface-erosion breakage model would occur in such flocs. In addition, such broken flocs combine with residual particles to reduce the residual turbidity. As a result of above mentioned processes higher flocculation index (FI) and lower residual turbidity can be achieved.

Besides the charge neutrality, sweep flocculation gives totally different results. In the case of sweep flocculation most of the particles are positively charged. Particles containing the opposite charges combine with each other to form aggregates. But these aggregates are not as compact as in the case of charge neutrality; instead they have branched structures. These aggregates show large fragment breakage model. The breakage of such flocs produces almost all positively charged particles which repel each other rather than combining with each other. As a result, residual turbidity increases in water with lower value of FI (Yu et al., 2009).

2.4.3 Coagulants Dose

The effect of particle charge, size and fractal dimension under different pre-coagulation pHs and alum dosages on microfiltration (MF) permeate flux and removal of humic acids (HAs) were studied by Wang, et al. in 2010. Both aggregate structure and size played important roles in membrane filtration. The study showed that under the optimum pre-coagulation alum dosages of 20 and 40 mg/L, the membrane fouling was decreased at pH 5 than pH 7 because the more loose aggregates formed under charge neutralization coagulation than sweep coagulation.

Another study was conducted by Wang et al. in 2008 to investigate the aggregates formed by inorganic monomer alum, polymer aluminium chlorohydrate (ACH) and polyaluminium chloride (PACl) and the effect of these coagulants on humic acid removal and microfiltration membrane fouling. Also the fractal dimension of flocs is studied against these coagulants and fractal dimension are higher for ACH and PACl as compared to monomer alum. The study shows that although ACH and PACl save 60-70% of coagulant dose in comparison to alum but these coagulants are not feasible for humic acid removal because they enhance the cake layer resistance two to three folds. So the results indicate that an optimum dose of alum based inorganic coagulants is adaptive for coagulation-MF hybrid process for organic removal (Wang et al., 2008).

2.4.4 Floc Fractal Dimension

Fractal dimension is a term coined by Mandlebrot in 1975. Nowadays, fractal dimension is used as a metric of the floc structure. Objects with random structure may be characterized using fractal dimension. Most of the particles which aggregate in natural and engineering systems are fractals.

According to the literature different coagulation conditions can bring changes in aggregate size and its fractal dimensions. However, it's very hard to separate the size effect from structure effect (Cho et al., 2005). It is now believed that fractal theories for particles aggregates can present a new quantitative method to describe the structure of particle aggregates in different water treatment systems (Lee et al., 2002).The important parameter for the measurement of fractal geometry, is to identify the difference in scale as a measure to describe structures. The relationship between the mass (M) and the size (R) of the fractal aggregate is:

$$M \propto R^{D_F} \qquad\qquad (i)$$

where D_F is the mass fractal dimension, and its values ranges between 1 and 3 in three dimensional space (Bushell et al., 2002). More compact and tightly packed aggregates have high fractal dimensions, while loosely arranged and highly branched structures have low fractal dimensions. Light scattering, settling and image analysis are the three most commonly used techniques to measure the fractal dimensions of aggregates (Koen and Willy, 1997; Wu et al., 2002; Tang et al., 2002; Chakraborti et al., 2003).

a) Fractal Measurement Using Light Scattering Technique

In most of the cases for elucidation of the structural properties of larger aggregates, small angle light scattering technique can be used. Using such advancements allow us to get the quick and non-intrusive structural information of particulate aggregates. A better mechanistic understanding of individual processes and on-line process control can be achieved using this technique. When a suspension of particles containing polarizable electrons is hit by a beam of light with an intensity of I_0 a portion of the light may be scattered with the intensity of the scattered light at any angle θ and at any given time. The properties of this scattered light dependent on the wavelength of the incident light, the size, shape and optical properties of the scattering particles, also the angle of observation and the positions of the dipoles. Small particles scatter light at large angles while large particles scatter light at small angles (Waite, 1999).

b) Fractal Measurement Using Image Analysis

To study the floc structural characteristics the most economical and useful technique is microscopy. Using microscope one can analyze individual aggregates easily on high magnification. Such a technique avoids the underestimation of floc structure by measuring only the solid area but not the effective area including pores and water in the body of the floc. Although this technique is painstaking but is still being utilized in many studies (Xiao et al., 2009). Fractal dimension of aggregates can also be done using direct microscopic observations. For this, the mass or number of particles are used at different length scales to relate the scaling properties of fractal objects. At times a suspension having aggregates of different sizes represent samples of the same

fractal object at different length scales. Here the number of particles in aggregates of different sizes but equal fractal dimensions can be related to the fractal dimension as (Eq. ii)

$$N \sim R_g^D \qquad \text{(ii)}$$

Where N represents the total number of units forming the clusters and R_g is the aggregate's radius of gyration. Fractal dimension of latex (Adachi and Ooi et al., 1990) and bacterial aggregates can be estimated by measuring R_g and counting N. We can use the projected image of an individual floc to measure its fractal dimension by relating the projected surface area of floc to its radius as

$$A \sim R^{D2} \qquad \text{(iii)}$$

Where D_2 is the fractal dimension of a two-dimensional projection of the object (Thill et al., 1998). The fractal dimension of the projection of an aggregate with a fractal dimension D in three dimensions is hypothetically linked to D_2 as

$$D_2 = D \ \text{ if } D \leq 2 \qquad \text{(iv)}$$

$$D_2 = 2 \ \text{ if } D > 2 \qquad \text{(v)}$$

2.5 COLLOIDAL AGGREGATION MODELS

Aerosol growth, colloidal aggregation and droplet formation are the natural systems for the aggregation of colloidal particles. Aggregation phenomena are widely being practiced not only in pure science but also in industries where paints, polymers and other biological materials are synthesized accordingly. When we talk about colloidal

aggregation literature reported two irreversible aggregation regimes: diffusion-limited aggregation (DLA) and reaction limited aggregation (RLA) (Odriozola et al., 2001).

2.5.1   Diffusion Limited Aggregation (DLA)

In diffusion limited aggregation Brownian motion is responsible for colloids aggregation and large aggregates formed when colloids collide with each other (Odriozola et al., 2001).

2.5.2   Reaction Limited Aggregation (RLA)

Reaction limited aggregation occurs when every collision does not lead to the formation of a new bond. More likely a number of collisions are required so that the particles can stick to each other and form the bond (Odriozola et al., 2001).

2.6 MEMBRANE FILTRATION

Currently, membrane filtration is being applied on large scale as advanced treatment technology for water treatment and particularly for the removal of particulate matter, turbidity, natural organic matter and sometimes for the removal of microorganisms. Because of the fact that membranes are very effective in removing pathogens and other contaminations from the water the use of membrane filtration is increasing in treatment of water but the high capital and operating cost of membranes is still a limiting factor in their widespread use (Mallevialle et al.,1996). To determine these costs important factors are the extent of permeate flux and frequency of membrane cleaning (Waite et al., 1999). In recent times, membrane filtration is combined with various physico-chemical processes to improve its effectiveness and to get good

results. Among these processes coagulation is considered to be a better option to combine with membrane filtration for the removal of particulate matter especially for turbidity removal. Pre-coagulated raw water has better filtration efficiency and also reduces the cake layer resistance of membrane. However, coagulation conditions and characteristics of particulate matter present in raw water largely affect the filterability in coagulation-MF system (Cho et al., 2005).

2.6.1 Membrane Filtration Parameters

The permeate flux J of a fluid across a clean membrane can be described using Darcy's law, i.e.,

$$J = \frac{\Delta P}{\mu R_{\mathrm{m}}} \qquad\qquad (vi)$$

where ΔP (Pa) is the pressure drop across the membrane, μ (kg/m/s) is the absolute viscosity of the permeating fluid, and R_{m} (1/m) is the hydraulic resistance of the membrane. Permeate flux can decrease because of the deposition of materials (i) inside the membrane pores due to adsorption or blocking processes, (ii) on the surface of the membrane in the form of a porous cake or gel, and (iii) in the form of a concentration boundary layer near the surface of membrane (Weisner and Aptel 1996). Resistance of cake layer (R_{c}) to permeate flux is increased when the reduction in pore size and blockage of pores occur because of the accumulation of materials in the form of a cake. Additional membrane resistance to permeation can be due to the concentration polarization phenomenon (R_{cp}). The feed water quality and the characteristics of mass transfer in the membrane module are the factors which determine the composition and

thickness of each layer of accumulated material on membrane. The composition and thickness of accumulated material on membrane are responsible for the changes in membrane resistances. Normally in water and wastewater treatment it has been observed that concentration-polarization layer, if formed produces very negligible resistance to permeate flux. So when talking about the membrane resistance the R_{cp} can be neglected because of its very small value. Therefore, the flux of a UF membrane having an accumulated material layer can be written as:

$$J = \frac{\Delta P}{\mu(R_m + R_c)} \qquad \text{(viiii)}$$

The resistance of cake solids according to filtration theory (Bowen and Jenner, 1995) may be written as:

$$Rc = \alpha \frac{m_p}{A_m} \qquad \text{(ix)}$$

In this equation m_p is the mass of deposited particles, α is the specific resistance of deposited material, which can be approximated for cakes formed from uniform, spherical particles using the Carman-Kozeny relationship, and area of the membrane is A_m:

$$\alpha = \frac{180(1-\epsilon)}{\rho_p dp^2 \epsilon^3} \qquad \text{(x)}$$

Where ϵ isthe void volume of the cake, the density of the particles is ρ_p , and mean diameter of the particles is d_p. The resistance of the cake produced in such condition

will be proportional to increase in cake mass and inversely proportional to the square of the primary particle size. Cake porosity also influences the α very strongly, for example, a 10 fold increase in α is expected with a change in ϵ from 0.2 to 0.1(Waite et al., 1999).

2.7 STEPS IN MEMBRANE FOULING

Membrane fouling occurs in a sequence of steps starting from pore narrowing and blocking of membrane (R_p), formation of gel layer and cake layer deposition (R_c). The initial stages of membrane pore narrowing and blocking are generally termed as foulant invasion and its addition into the membrane volume. This stage not only leads to physical irremovable fouling of membrane (Meng et al., 2009) but is also measured as footstone of consequent fouling progress. Adsorptive fouling on the surface of membrane is the major source of membrane pore blocking especially when the size of foulants are less than the membrane pore size (Huang et al., 2010).

2.7.1 Coagulation and Membrane Fouling

A number of parameters are involved in coagulation process i.e. fluid mechanical environment and velocity gradient lead the formation of aggregates with different shape and fractal dimension (Lee et al., 2000; Carroll et al., 2000). Such variations in coagulation parameters finally produce the flocs of different size and fractal properties and it becomes difficult to separate their effect on membrane fouling. On same cake layer accumulation rate, flocs produced by higher aggregation conditions have high specific cake layer resistance that flocs generated at low aggregation conditions

(Logan and Kilps, 1995). Filtration efficiency of MF is affected by coagulation mechanisms with varying coagulant dose and pH of raw water (Lee et al., 2000). The quantity, characteristics and type of natural organic matter (NOM) in raw water has high influence on membrane fouling (Carroll et al., 2000).

Membrane fouling is largely affected by the characteristics of aggregates or flocs formed through coagulation. Aggregate properties can be visualized by a number of critical parameters i.e. aggregate sizes, fractal dimensions and charge on aggregates (Wang et al., 2010).

2.8 MATHEMATICAL APPROACH FOR CLAY FLOCS

In this section we introduce the notion of fractal dimension and equations that connect microstructural characteristics of a membrane cake with its permeability. We then propose a method for estimating the fractal dimension of a growing membrane cake based on variables that can be easily measured in a filtration experiment.

2.8.1   Fractal Dimension of a Membrane Cake

The fractal dimension, D_{cake}, of a growing deposit defines how its average thickness scales with the number of deposited particles, N (Meakin, 1984; Vicsek, 1992):

$$L \sim N^{\varphi} = N^{\frac{1}{D_{cake}-2}},$$
(xi)

where φ is the scaling exponent and $D_{cake} = 2 + \dfrac{1}{\varphi}$ is the fractal dimension of the deposit.   Equation (xi) has been used to describe and quantitatively differentiate

morphologies of deposits formed under conditions characterized by a broad range of

particle Peclet numbers (Kozeny, 1927) and particle-particle interaction energies

(Tarabara et al., 2002). The number of particles in the deposit, N, is proportional to

its mass, M. In filtration with complete rejection and no back-transport of particles,

the mass of deposit equals the product of feed concentration of particles, C_f, and

permeate volume, V_p. Thus, when C_f is constant, N is proportional to the permeate

volume and eq. (xi) can be rewritten as

$$L \sim V_p^\varphi \qquad \text{(xii)}$$

The average thickness of the cake, L, is given by:

$$L = \frac{C_f V_p}{A_m (1-\varepsilon) \rho_s} , \qquad \text{(xiii)}$$

where ρ_s is particle density, ε is porosity of the cake, and A_m is the area of the

membrane. Combining eqs. (xii) and (xiii) yields a simple scaling relationship:

$$\ln(1-\varepsilon) \sim (1-\varphi) \ln V_p \qquad \text{(xiv)}$$

or

$$\ln(1-\varepsilon) \sim \frac{D_{cake}-3}{D_{cake}-2} \ln V_p . \qquad \text{(xv)}$$

When the values of permeate flow rate and cake porosity as functions of filtration time are known, eq. (xv) can be used to determine D_{cake}. To our knowledge, this scaling relationship has not been described in the published literature.

2.8.2 Specific Hydraulic Resistance of a Membrane Cake

In the absence of an osmotic pressure difference across the membrane, the volumetric permeate flux is given by:

$$j = \frac{\Delta P}{\mu(R_m + R_c)},$$

(xvi)

where ΔP is the transmembrane pressure differential, μ is viscosity of the permeating fluid, while R_m and R_c are hydraulic resistances of the unfouled membrane and the membrane cake, respectively. Specific hydraulic resistance of a membrane cake of thickness L is defined as

$$\hat{R}_c = \frac{R_c}{L}$$

(xvii)

and can be connected to microstructural properties of the cake using one of the permeability models (see section 2.3).

In early studies of cake filtration, Ruth and co-workers (Ruth et al., 1933; Carman, 1937) and Carman (Ruth et al., 1933; Carman, 1933; Carman, 1934) introduced mass-based specific cake resistance defined as the cake's hydraulic resistance R_c per unit mass of the cake and per unit surface area of the filter (Carman, 1934):

$$\alpha_M = \frac{A_m}{M} R_c, \qquad \text{(xviii)}$$

where ρ is density of the cake and M is cake's mass. Comparison of definitions (xvii) and (xviii) shows that specific hydraulic resistances $\hat{R}_c$ and α_M are related via cake density, ρ :

$$\alpha_M = \frac{\hat{R}_c}{\rho} \qquad \text{(xix)}$$

Combining (xvi) and (xviii) and assuming $M = C_f V_p$ gives an expression for α_M in terms of values that can be easily measured in a filtration experiment:

$$\alpha_M = \frac{A_m}{C_f V_p} \left(\frac{\Delta P}{j\mu} - R_m \right). \qquad \text{(xx)}$$

Equation (xx) can be used to determine the dependence of mass-based specific cake resistance α_M on the filtration time based on experimental measurements of permeate volume as a function of time.

One should note that equating the cake mass to $C_f V_p$ is based on two assumptions: that all particles are rejected by the membrane and that there is no back-transport of particles away from the membrane surface. Under these conditions all particles that approach the membrane deposit on it to form the cake. It is also assumed that the concentration of particles in the feed suspension is constant throughout the filtration experiment.

41

2.8.3 Estimating Porosity of a Membrane Cake Based on Experimental Values of Permeate Flux and a Permeability Model

2.8.3.1 Estimation of Cake Porosity Based on Carman-Kozeny Model

The Carman-Kozeny equation (Lai, et al., 1975; Ripperger et al., 2012) states that the specific hydraulic resistance of a membrane cake is given by:

$$\hat{R}_c^{CK} = K_K \frac{s^2}{\varepsilon^3}, \tag{xxi}$$

where K_K is Kozeny constant and s is specific surface area of the cake

Noting that cake density, ρ, and cake porosity, ε, are connected via the density of the particles, ρ_s, as $\rho = \rho_s(1-\varepsilon)$, one can combine eqs. (xxi) and (xix) to express the mass-based specific cake resistance as a function of microstructural properties of the cake:

$$\alpha_M^{CK} = K_K \frac{s^2}{\rho_s} \frac{1}{\varepsilon^3(1-\varepsilon)} \tag{xxii}$$

With α_M values available from filtration experiments (see eq. (xx)), eq. (xxii) can be used to get a Carman-Kozeny model based estimate of the average cake porosity, ε, as a function of filtration time. This is done by combining eqs. (xx) and (xxii):

$$\frac{A_m}{C_f V_p}\left(\frac{\Delta P}{j\mu} - R_m\right) = K_K \frac{s^2}{\rho_s} \frac{1}{\varepsilon^3(1-\varepsilon)} \tag{xxiii}$$

And using porosity as the fitting parameter to balance eq. (xxiii).

With the values of ε known, eq. (xv) can be used to determine D_{cake}.

2.9 MATHEMATICAL APPROACH FOR HUMIC ACID FLOCS

The approach for humic acid flocs is same as for clay flocs except a little change in calculating the porosity of membrane cake. In case of humic acid flocs membrane cake porosity was measured by Carman-Kozeny model and also by Happel model.

2.9.1 Estimating Porosity of Membrane Cake Based on Experimental Values of Permeate Flux and a Permeability Model

2.9.1.1 Estimation of Cake Porosity Based on Carman-Kozeny Model

Equation (xx) can be used to determine the dependence of mass-based specific cake resistance α_m on the filtration time based on experimental measurements of permeate volume as a function of time. Noting that cake density, ρ, and cake porosity, ε, are connected via the density of the particles, ρ_s, as $\rho = \rho_s(1-\varepsilon)$, one can combine eqs. (xvii) and (xviii) to express the mass-based specific cake resistance as a function of microstructural properties of the cake:

$$\alpha_m = K_K \frac{s^2}{\rho_s} \frac{1}{\varepsilon^3(1-\varepsilon)} \qquad \text{(xxiv)}$$

In the assumption that the cake consists of spherical particles of the same size (d_c), sphericity and Kozeny constant are equal to 1 and 5, respectively, and eq. can be rewritten as

$$\alpha_m = 180 \frac{1}{\rho_s d_c^2} \frac{1-\varepsilon}{\varepsilon^3} . \qquad \text{(xxv)}$$

With α_m values available from filtration experiments (see eq. (xx)), eq. (xxv) can be used to determine average cake porosity, ε as a function of filtration time. With the values of ε known, eq. (xv) can be used to determine the fractal dimension of the membrane cake.

2.9.2 Estimation of Cake Porosity: Happel Model

The Carman-Kozeny model was found to produce unrealistic predictions of settling velocity of fractal aggregates (Veerapaneni and Weisner, 1996), and it was suggested that other permeability models such as Brinkman or Happel models should be used to describe permeability of fractal objects (Wang et al., 2010). According to the Happel model (Zhan et al., 2011)

$$\hat{R}_c^H = \frac{18}{d_c^2} \frac{\gamma^3 \left(3 + 2\gamma^5 \right)}{3 - 4.5\gamma + 4.5\gamma^5 - 3\gamma^6} , \qquad \text{(xxvi)}$$

where $\gamma = \left(1 - \varepsilon \right)^{1/3}$.

Applying eq. (xix):

$$\alpha_M^H = \frac{\hat{R}_c^H}{\rho_s \left(1 - \varepsilon \right)} = \frac{18}{d_c^2 \rho_s} \frac{3 + 2\gamma^5}{3 - 4.5\gamma + 4.5\gamma^5 - 3\gamma^6} . \qquad \text{(xxvii)}$$

Equation (11) can be used to get a Happel model based estimate of the average cake porosity, ε as a function of filtration time. This is done by following the same

procedure as described in section 2.3.1 - by using porosity as the fitting parameter to ensure that eq. (xx) and eq. (xxvii) give the same value of the mass-based specific cake resistance.

METHODOLOGY

This chapter describes the experimental plan, equipment utilized for experimental work, steps of methodology and the data analysis techniques. In this study two synthetic feed solutions were prepared and tested against different alum doses and various Gt_{mix} conditions. The methodology has been divided into two sections. Section (A) and section (B) are representing the clay and humic acid synthetic feed solutions respectively. According to the nature and objectives of the study, the experimental plan for each section has been divided into two phases. In Phase-I of each section, the effect of alum dose, pH and rapid mix velocity gradient (Gt_{mix}) on floc size, shape and fractal dimension were studied in detail. Phase-II followed the results of Phase-I and the effect of these flocs formed by rapid mix conditions on membrane filtration, cake formation, membrane resistance (R_c) and specific cake resistance (α_m) were studied.

3.1 EQUIPMENTS AND INSTRUMENTS

The equipments and instruments utilized in this study are described below.

3.1.1   Jar Test Apparatus (Model 7790-400, Phipps & Birds)

A jar test apparatus (Model 7790-400, Phipps & Birds) was utilized for coagulation/flocculation experiments. The multiple stirrers with reproducible stirring speeds allowed standard conditions for the tests to be adopted, a basic requirement in order to obtain reliable results. Jar test apparatus was used for the determination of

optimum coagulant dose, mixing conditions and pH required for the removal of solid particles from the water.

3.1.2   TOC Analyzer

TOC analyzer used for this study was Total organic carbon analyzer (OI Analytical model 1010 Analyzer, College Station, TX). In TOC analyzer total combustion of samples by heating them at $680^{\circ}C$ is done in an oxygen rich environment inside TC combustion tubes filled with a platinum catalyst followed the combustion catalytic oxidation method. A simple principle of oxidation through heating and combustion is utilized in this method so pretreatment and post-treatment using oxidizing agents are unnecessary. An infrared gas analyzer (NDIR) was used to detect the carbon dioxide generated in oxidation.

3.1.3   pH Meter

A pH meter was used to read the acidic or alkaline values of a liquid. The pH meter works on the simple principle to measure the concentration of hydrogen ions in water. When acids dissolve in water they form positively charged hydrogen ions (H+). More of positively charged hydrogen ions in a liquid means the acid is stronger. On the other hand alkali or bases when dissolve in water they produce negatively charged hydrogen ions (-OH). Similarly more of negatively charged hydrogen ions in a liquid means the base is stronger.

3.1.4 Particle Size Analyzer

Mastersizer is an instrument that works on the principle of laser diffraction to measure the particle size. As a laser beam passes through a suspended particulate sample, laser diffraction measures the particle size distributions by measuring the angular variation in intensity of light scattered. In particulate distribution small particles distribute light at large angles relative to the laser beam and large particles distribute light at small angles. Using the Mie theory of light scattering the angular scattering intensity data is then analyzed to calculate the size of the particles responsible for creating the scattering pattern (Waite, 1999; Sorensen, 2001). The particle size is normally reported as a volume equivalent sphere diameter. In this study a Malvern Mastersizer 2000 was used to study the floc characteristics.

3.1.5 Turbidimeter (Hach 2100N)

A turbidimeter of model Hach 2100N was used to measure the turbidity of synthetic water. Turbidimeter also works on the principle of light scattering. A light beam will remain undisturbed when passed through pure water. But if the water has suspended particles, the light distortion will occur. The light beam interacts with the suspended particles and these particles absorb the energy and re-radiate light in all directions. This re-radiated light is detected by the photo-detector and gives turbidity values.

3.1.6 Confocal Light Microscope

The confocal laser scanning microscope used this study was Zeiss LSM 5 Pascal with an Argon laser ($\lambda = 488$nm) worked as the light source. In confocal laser scanning

microscopy, light beam passes through an aperture and an objective lens is used to focus the light on small volume within or on the surface of the specimen. Scattered and reflected light from the specimen is then re-collected by the objective lens. The light intensity is detected by photodetector after passing through a pinhole. This light signal is converted into electrical one to be recorded by the computer.

3.1.7   Membrane Filtration Assembly

Membrane filtration assembly contains an amicon 8050 membrane filtration cell of 50mL. A 5L pressurized vessel (UM-Alloy Products corp. 140 PSI) modified for continuous stirring during the filtration experiments (Figure 3-7). A compressed air gas tank with air regulator (Victor Equipment Company) and filtration tubing of Mazzerpollo made (Figure 3-5) were used in membrane filtration assembly. Membrane used in all experiments to filter floc suspension was Ultrafiltration polyethersulfone membrane (50 kDa MWCO, Pall).
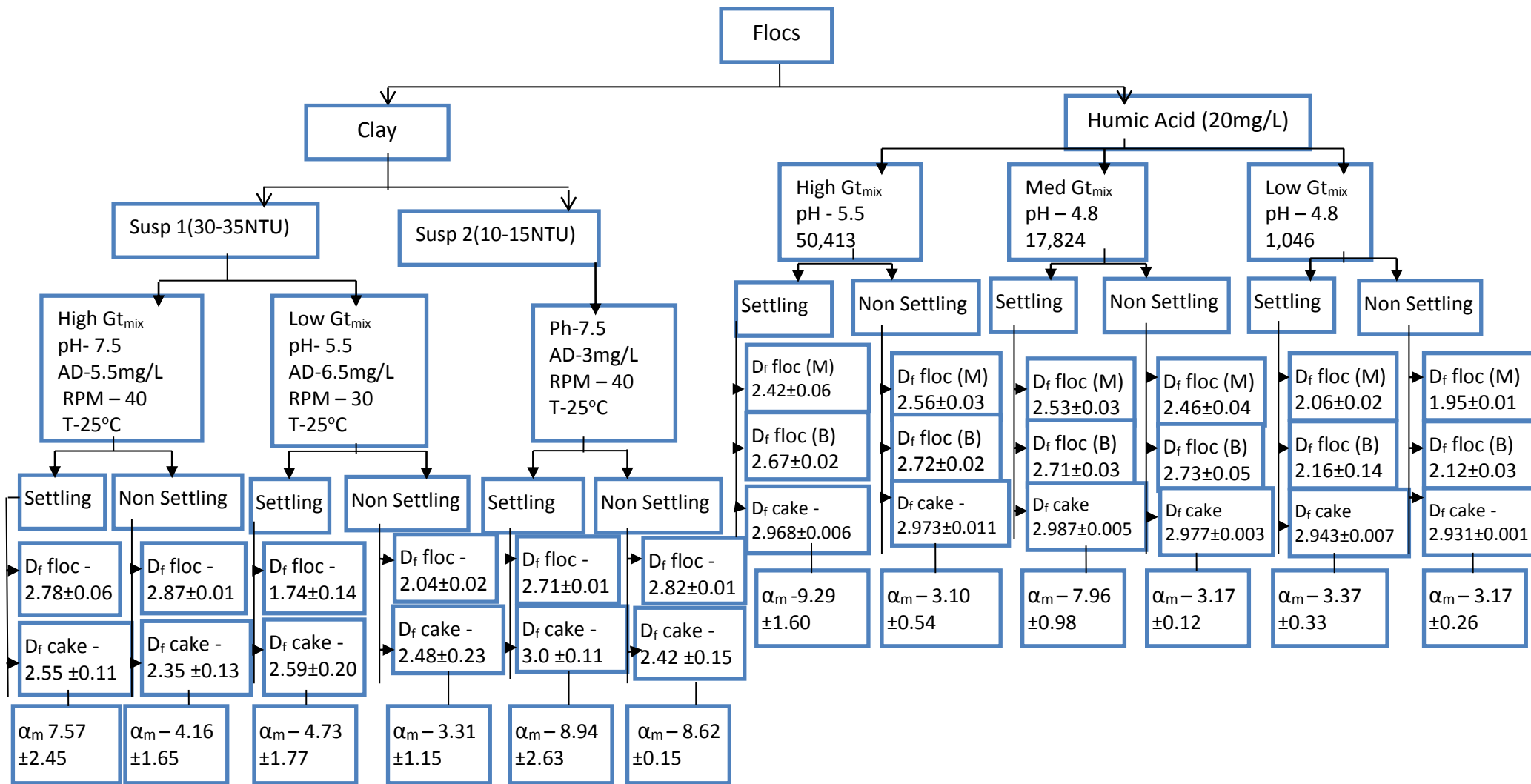
Figure 3-1: Flow chart of experiments under Phase I and Phase II
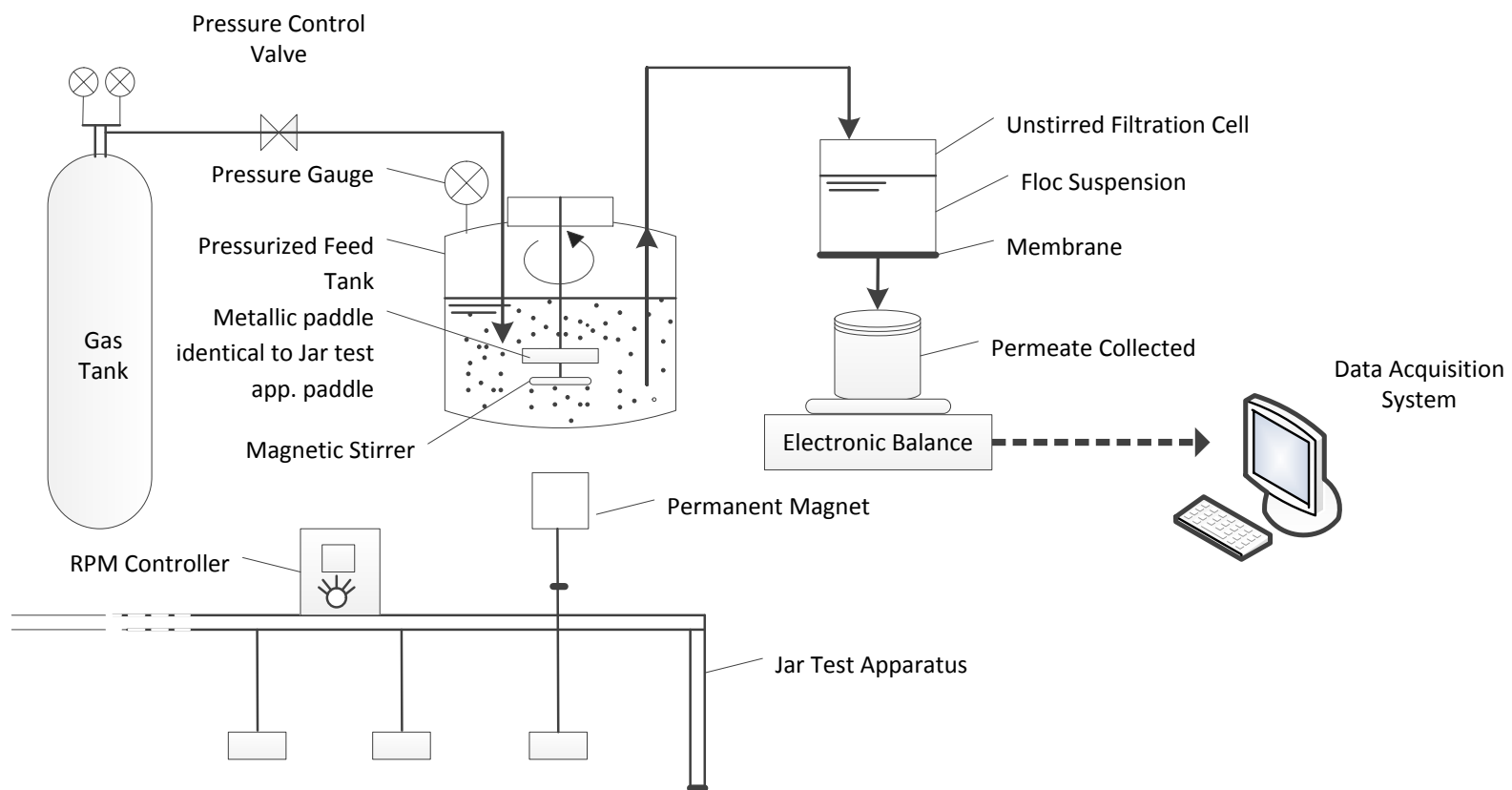
Figure 3-2: Schematic diagram of the experimental apparatus.

3.2 EXPERIMENTS WITH CLAY (SECTION A)

3.2.1 Phase-I: Determining the effect of coagulation parameters on floc characteristics

3.2.1.1 Feed Water Preparation

Two types of synthetic feed water were used in this study.

3.2.1.1.1 Synthetic Feed Water Ia – Clay Suspension

A synthetic suspension of kaolin clay supplied by (Spectrum Chemicals) was prepared.

This synthetic feed water suspension was prepared in deionized water, as suggested by

Yukselen and Gregory (Yukselen and Gregory, 2004). To prepare the stock solution, 3

g of kaolin clay was dissolved in 1L deionized water Figure 3-3a. After 30-min mixing

on 300 rpm, the suspension was allowed to settle down for 24 h at room temperature

(Figure 3-3b). After 24 h settling top 800mL of suspension was decanted in a separate

beaker and was further diluted by adding deionized water to reach a final turbidity

range of 30-35 NTU. According to literature water having a turbidity range of 30-35 is

termed as medium turbid water. That's why a medium turbid water was chosen for this

study. The turbidity value was measured using turbiditimeter. The pH of the synthetic

feed water was adjusted to 8.7 $\pm$ 0.1 by adding 0.1M NaOH. Particle size distribution

of synthetic clay suspension was measured as d_{90}= 0.98 μmby using laser light

scattering (Malvern Mastersizer 2000, Malvern, UK) (Mendret et al., 2009).
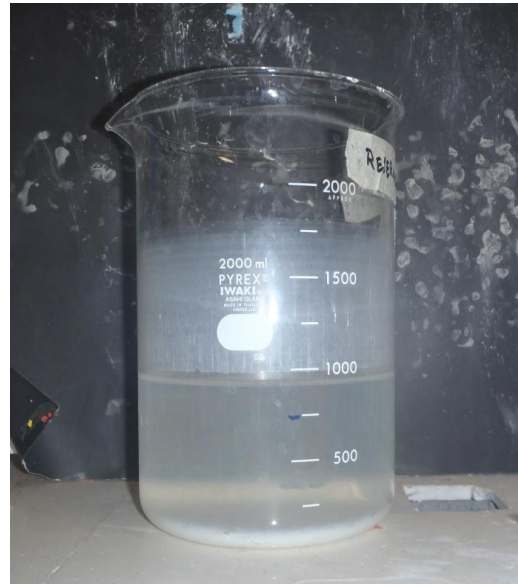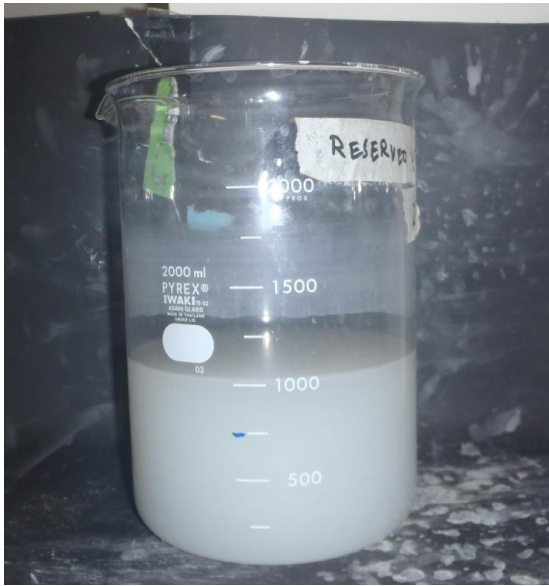
Figure 3-3a: Clay suspension after 30 min mixing

Figure 3-3b: Clay suspension after 24 hrs of settling

3.2.1.1.2   Synthetic Feed Water Ib – Clay Suspension:

The same stock solution of kaolin clay which was previously used is further diluted by adding deionized water to attain the resultant turbidity of 10-15 NTU. The pH of low turbidity synthetic feed water was adjusted to 8.50 ± 0.1 by adding 0.1M NaOH.

3.2.1.2 Reagents Preparation

Aluminum sulfate (alum, $Al_2(SO_4)_3 \cdot 18H_2O$, reagent grade, Sigma Aldrich) was used as the principle coagulant. The stock alum solution was prepared by dissolving 1g of alum in 1L of deionized water (Wang et al., 2007). A 0.1M NaOH solution was prepared by dissolving 3.399g in 1L of DI water.

3.2.1.3 Optimum Coagulant Dose Determination

Alum salt was used as principal coagulant in this study for the formation of colloidal aggregates. Coagulation experiments were performed using a jar test apparatus (Model 7790-400, Phipps & Birds). Optimum coagulant dose was determined using six 2L cylindrical glass beakers to provide the maximum mixing conditions in the beakers. 1L of synthetic feed water having a turbidity of 30-35 NTU prepared by clay suspension was poured in 2L glass beakers to determine the optimum coagulant dose Figure 3-4. To determine the coagulant dose, required amounts of alum doses were added to the measuring beakers. These six beakers were fixed in a wooden stand to add all dosages at the same time to avoid the difference in reaction time. For optimum dose determination alum doses in a range of 2-44 mg/L were tested.

For medium turbidity water of 30-35 NTU, the rapid mixing of 200 rpm was provided for 1 min to thoroughly mix the synthetic feed suspension and coagulant in the beaker. Slow mixing at a speed of 40 rpm was provided for 20 min and the suspension was allowed to settle for 30 min. After 30 min of settling, a sample of 30 mL was collected using a micropipette approximately 2 cm below the surface of water in the beaker. This sample was then tested for remaining turbidity using turbiditimeter (Hach 2100N).
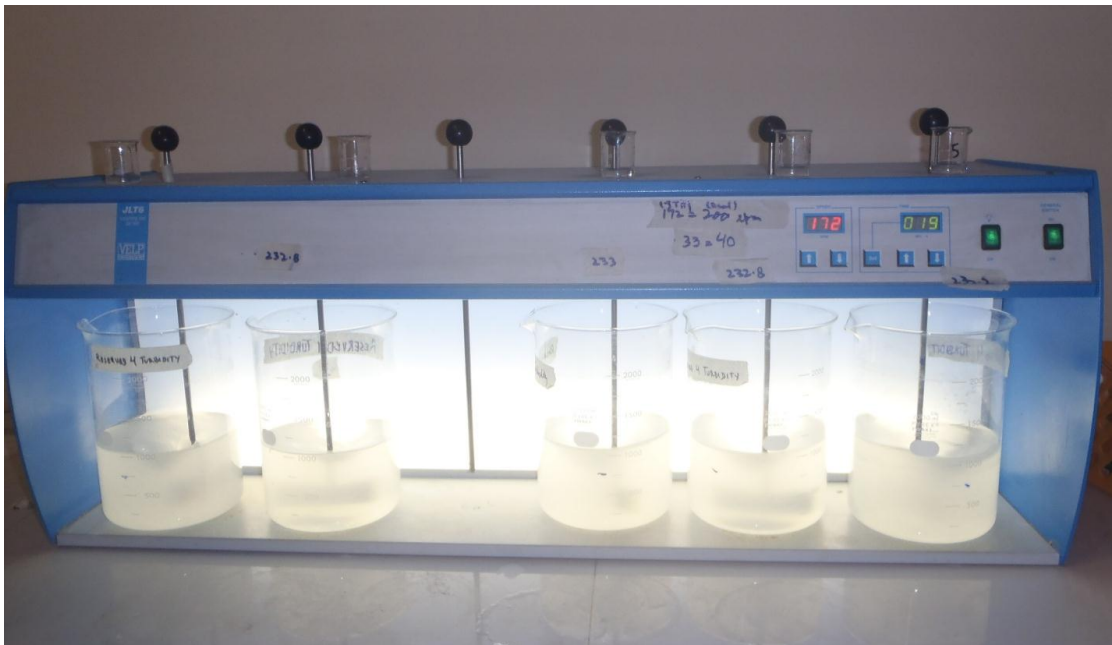
Figure 3-4: Coagulant dose determination for clay synthetic feed water

For low turbidity water of 10-15 NTU, the coagulation/flocculation conditions were same as medium turbidity water. The only exception was optimum coagulant dose range. For low turbidity water (10-15 NTU), the dosage range from 1-5 mg/l was tested. The temperature of both feed suspensions (10-15 & 30-35 NTU) was kept constant at $25 \pm 1^{\circ}C$ in all experiments (Li et al., 2006; Wang et al., 2007).

3.2.1.4 Floc Formation Study

A continuous flow laser diffraction instrument (Malvern Mastersizer 2000, Malvern) was used in a modified jar test apparatus to study the coagulation and flocs formation phenomenon (Figure 3-5a). Mastersizer was used for measurement of floc size formed during floc growth. For this a sample from beaker remained circulating through transparent plastic tubing of 5 mm ID by means of a peristaltic pump (Model no. 7520-

00, Masterflux, Cole-Palmer) installed downstream from the Mastersizerat, at a flow rate of 25 ml/min with recycling back to the beaker. To prevent the aggregate breakage, the peristaltic pump was applied after the Mastersizer instrument. The Mastersizer was programmed to measure floc size and structure after every 30s for the entire flocculation duration (Li et al., 2006).
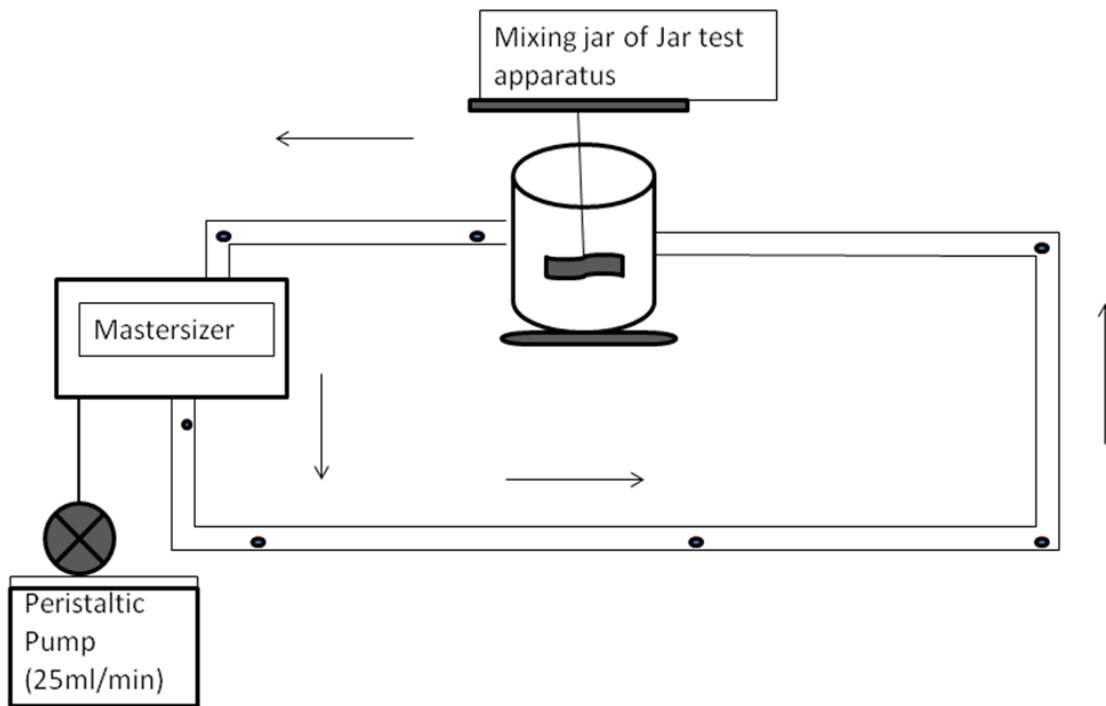
Figure 3-5a: Experimental set up for floc size and fractal dimension measurement
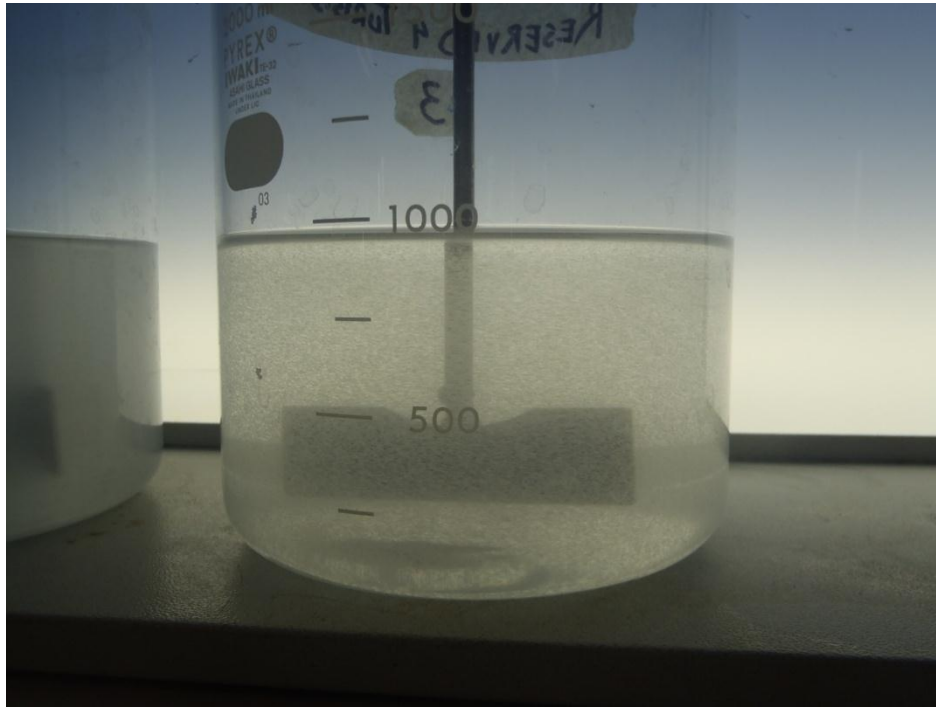
Figure 3-5b: Clay flocs formation by addition of aluminum sulfate coagulant

To study the variations in floc size and structure (D_f) two different coagulation/flocculation conditions were tested for medium turbidity water (30-35NTU).

A high $\bar{G}t_{mix}$ aggregation condition was maintained at pH 7.5, alum dose of 5.5 mg/L and slow mixing @ 40 rpm and a low $\bar{G}t_{mix}$ aggregation condition was induced at pH 5.5, an alum dosage of 6.5 mg/L and slow mixing @ 30 rpm. These mixing conditions were selected with aiming a significant different in floc fractal dimension. Difference in floc structures (D_f) were confirmed based upon the measurements of fractal dimensions using Box Counting method. Confocal microscopic images of flocs were

used for box counting (Thill et al., 1999). For low turbidity water (10-15NTU) the coagulation and flocculation was performed on only high mixing conditions.

3.2.1.5 Determination of Fractal Dimension

3.2.1.5.1   Box Counting Using Floc Images

Fractal dimension of clay flocs was mesaured using confocal microscopy images. Clay flocs prepared as a result of flocculation were gently placed in 0.8 mm well (dip) microscopic glass slides. Glass cover slips of 22mm x 22mm were used to cover the well of slides and sealed with nail polish to keep the flocs in wet conditions.

The confocal laser scanning microscope used for this study was Zeiss LSM 5 Pascal. Argon laser was used as light source with a wavelength of 488 nm. Images obtained from the confocal laser microscopy were stored in a tiff format of 1024×1024 pixels (3.00 MB).

The technique utilized for fractal measurements of floc images was Box Counting. In Box Counting algorithm images is covered with boxes of size d. Box size d is divided by 2 at every step and the number of boxes required to cover the complete structure is counted. If the structure is fractal the log (box counting) versus log (box size) gives a straight-lined curve. The slope of that curve is fractal dimension of image (Thill et al., 1998).

3.2.2 Phase-II: Major focus of this phase was to determining the effect of floc size and shape on membrane fouling, quality and quantity of permeate and flux decline.

3.2.2.1 Membrane Filtration

Membrane filtration experiments were performed using Amicon 8050 dead end cell (Millipore Corp.) connected to a 5 L pressurized feed reservoir. Membrane used to filter floc suspension was Ultrafiltration polyethersulfone membrane (50 kDa MWCO, Pall). Prior to each filtration experiment the membrane was compacted on a constant pressure of 50 psi using the DI water to get a steady permeate flux. The permeate flux was measured continually by recording the weight of the filtrate using an electronic balance (Digital balance AV8101C, Ohaus Corp.) (Figure 3-6) interfaced with a PC (Figure 3-7). Membrane fouling experiments were also performed on constant pressure mode for all experimental conditions. As the current study was aimed to study the cake growth and its characteristics, stirring was not provided in the membrane filtration cell to avoid the hindrance in cake layer deposition. Membrane filtration experiments were performed in triplicate for all six coagulation/flocculation experimental condition.
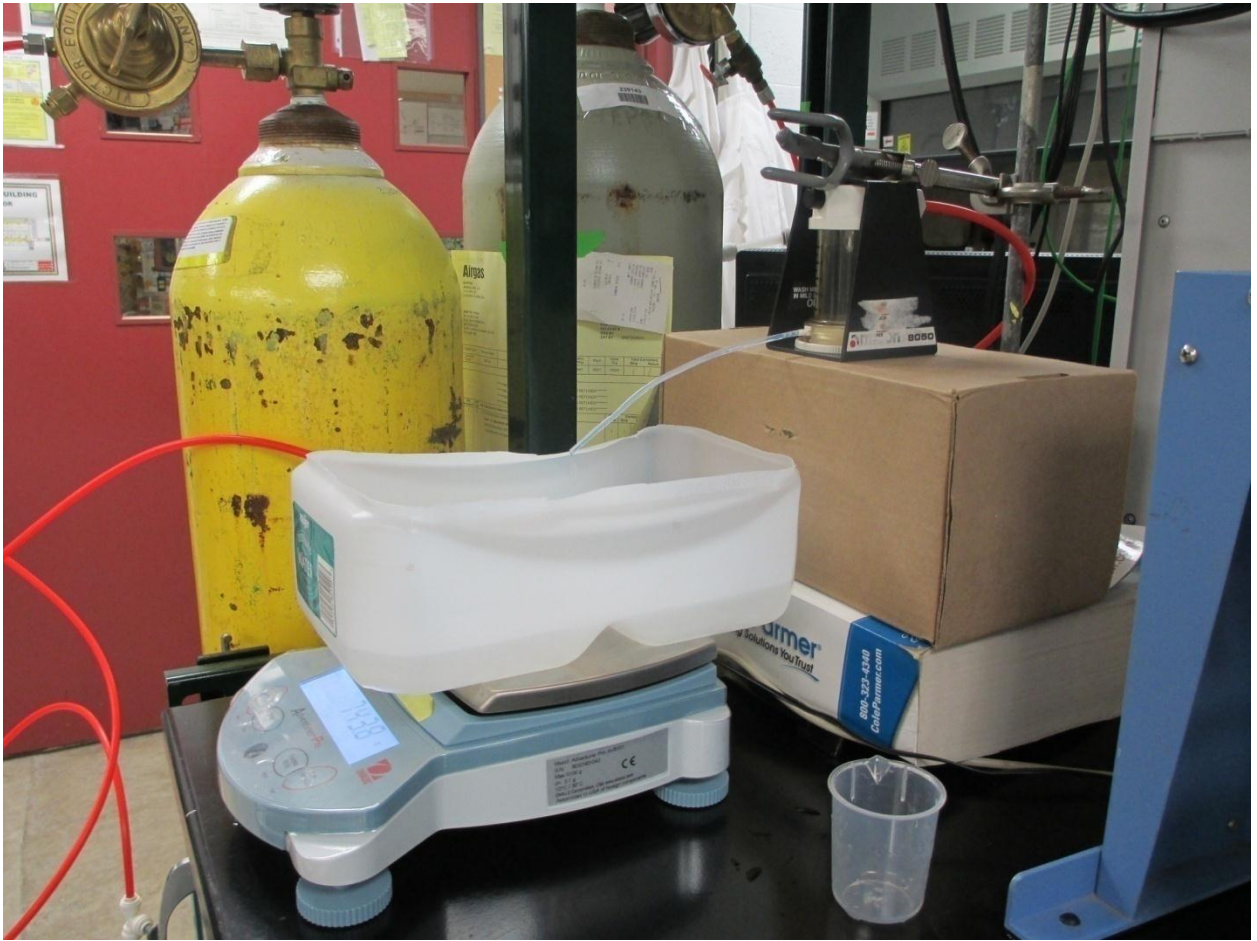
Figure 3-6: Permeate flux measurement by continually recording the weight of the filtrate using electronic balance
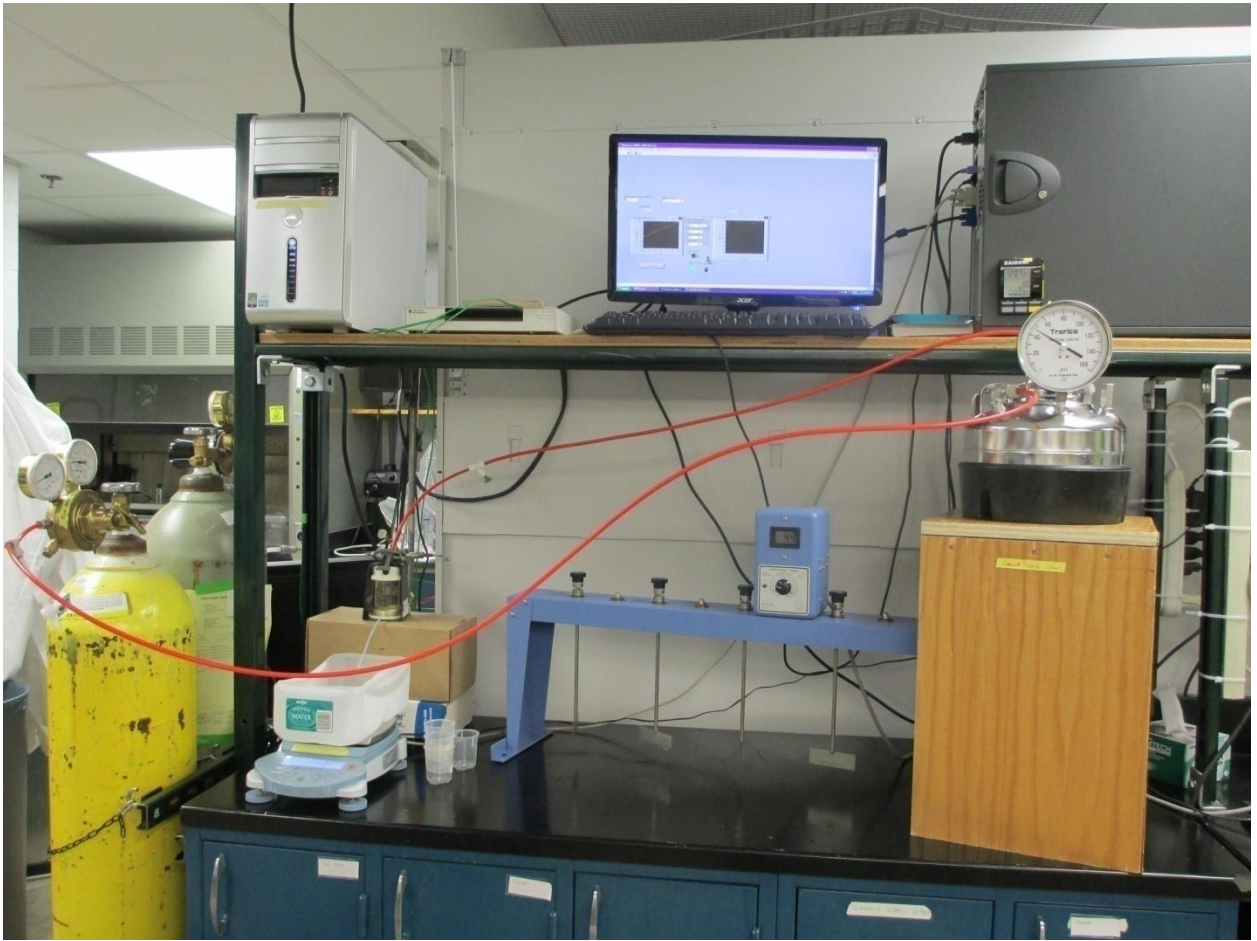
Figure 3-7: Membrane filtration set up

In all membrane filtration experiments 1.5 L of floc suspension was filtered through the PES membrane. To avoid the settling of flocs in the suspension with the passage of time and to filter a homogeneous floc suspension a continuous stirring was provided in the pressurized feed tank to keep the flocs in suspension (Figure 3-8 & 3-9). For that purpose a magnet was attached to one of jar test apparatus's paddle. A paddle equal to the size of jar test apparatus's paddle was constructed and kept suspended in the pressurized feed tank (Figure 3-9). A magnetic stirrer was attached to that paddle so that the paddle can move according to rotating speed of magnet attached with jar test

apparatus (Figure 3-8). Then in each membrane filtration experiment the floc suspension in pressurized feed reservoir was mixed on the respective rpm on which the floc suspension was produced during the flocculation.
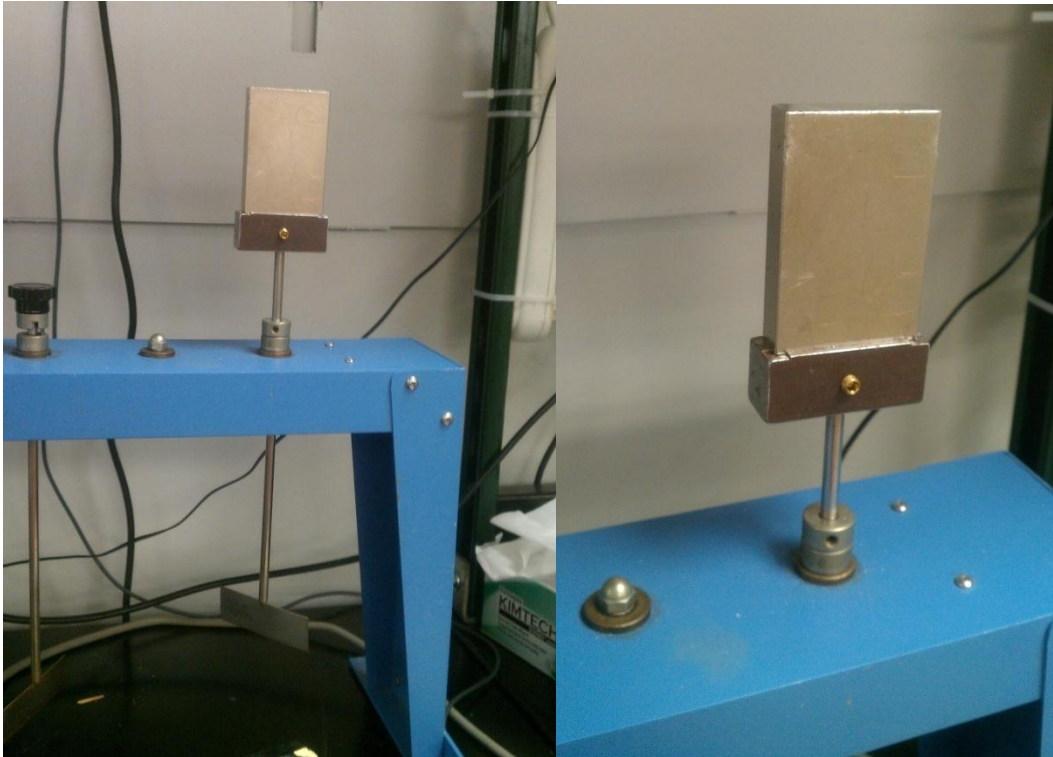
Figure 3-8: Magnet attached to one of the Jar test's paddle

Figure 3-9: Modified lid of pressurized feed reservoir having metallic paddle and magnetic stirrer

Two sets of membrane filtration experiments were performed for all clay coagulation/flocculation conditions. In one set of membrane filtration experiments flocs generated under high $\bar{G}t_{mix}$ and low $\bar{G}t_{mix}$ conditions and also flocs generated from low turbidity water are allowed to settle for 30min. After 30 min of settling the supernatant was transferred into the pressurized feed reservoir very carefully using a plastic tube of 5 mm ID for membrane filtration. A time of 30 min was provided to remove the settleable flocs to model the conventional filtration treatment process. In another set of membrane filtration experiments the flocs generated under high$\bar{G}t_{mix}$ and low $\bar{G}t_{mix}$ conditions and also flocs generated from low turbidity water were

transferred to pressurized feed reservoir for membrane filtration. No settling time was provided in these filtration experiments to model the direct filtration treatment process.

3.3 EXPERIMENTS WITH HUMIC ACID (SECTION B)

3.3.1 Phase I: Determining the effect of coagulation parameters on floc characteristics.

3.3.1.1 Synthetic Feed Water II – Humic Acid

To prepare synthetic feed water of humic acid, ultrapure water ($\sim$ 18 MΩ·cm^{-1}) supplied by Barnstead E-pure system was used. Stock solution of humic acid was prepared by dissolving 1g of Sodium Humate (MW 4,000 to 23,000 Da, Sigma-Aldrich) in 1L of ultrapure water for 3 days. The pH of humic acid stock solution was adjusted to 8.0 by adding 0.1 M HCl. After mixing of 3 days the humic acid stock solution was filtered through 0.45 μm nitrocellulose membrane (Millipore) and stored in the dark at 4°C. The concentration of humic acid in stock solution was measured by TOC analyzer which was in the range of 240 to 280 mg TOC/L. This humic acid stock solution was diluted to have a final concentration of 20 mg/L humic acid by using deionized water.

3.3.1.2 Reagents Preparation

Aluminum sulfate (Alum, $Al_2(SO_4)_3$. $18H_2O$, reagent grade, Sigma Aldrich) was used as the principle coagulant for humic acid coagulation/flocculation. The stock alum solution was prepared by dissolving 10g of alum in 1L of ultrapure water ($\sim$ 18 MΩ·cm^{-1}) (Wang et al., 2011). 2mM aqueous solution of $NaHCO_3$ was prepared by dissolving 16.8mg of $NaHCO_3$ in 100mL of ultrapure water.

3.3.1.3 Coagulant Dose Optimization

The coagulant dose was optimized for humic acid diluted stock solution of a concentration range of 27-32 mg (HA)/L on high $\bar{G}t_{mix}$ conditions which means the rapid mixing was provided for 1 min at 200rpm and slow mixing was provided for 20 min at 40rpm.

The pH of feed solution was adjusted to ~ 9.3 before coagulation. To find out the optimum coagulant dose for humic acid feed water, alum doses were tested in a range of 10-100 mg/L. The pH of feed solution was adjusted to 5.5 and 4.8 after addition of optimum coagulant dose for high $\bar{G}t_{mix}$ and medium to low $\bar{G}t_{mix}$ conditions respectively to generate the flocs of different D_f. After 20 min flocculation the floc suspension was allowed to settle for 30 min. A sample of 40mL was collected by a micropipette approximately 2 cm below the water surface and tested for humic acid content using TOC analyzer. The temperature of feed solution was maintained to 25 ± 0.5°C in all experiments.

3.3.1.4 Coagulation and Flocs Formation

For humic acid flocs formation three mixing ($\bar{G}t_{mix}$) conditions were tested, where $\bar{G}$ is the mean velocity gradient and t_{mix} is time of mixing. Here again the $\bar{G}t_{mix}$ conditions were planned aiming the flocs of different D_f (Table 3-1). The floc size and D_f study of humic acid flocs was carried out as explained in section (A).

Table 3-1: Evaluation of pretreatment processes.

Experiment code	Feed water humic acid content, mg(HA)/L	Pretreatment step 1: Coagulation			Pretreatment step 2: Flocculation			Pretreatment step 3: Settling	Total filterable solids[e] in the membrane feed, mg/L
		$\bar{G}t_{mix}$	Coagulant dosage, mg/L	pH	$\bar{G}$, s⁻¹	t_{mix}, s	$\bar{G}t_{mix}$	Settling time, min	
High$\bar{G}t_{mix}$→Settle[a]	19.7[c]	12,600[d]	70.0	5.5 ± 0.1	42.00	1,200	50,400	30	13.8 ± 7.7
High$\bar{G}t_{mix}$→Direct[b]					42.00		50,400	0	88.4 ± 0.0
Med$\bar{G}t_{mix}$→Settle[a]				4.8 ± 0.1	14.85		17,820	30	19.8 ± 1.0
Med$\bar{G}t_{mix}$→Direct[b]					14.85		17,820	0	88.4 ± 0.0
Low$\bar{G}t_{mix}$→Settle[a]					5.25	360	1,890	30	36.6 ± 3.7
Low$\bar{G}t_{mix}$→Direct[b]					5.25	360	1,890	0	53.8 ± 3.7

[a] Simulates the pretreatment train of a conventional filtration process: coagulation + flocculation + settling.

[b] Simulates the pretreatment train of a direct filtration process: coagulation + flocculation.

[c] Corresponds to 10 mg(TOC)/L.

[d] Corresponds to $\bar{G}$ = 210 s-1 and t_{mix} = 60 s.

[e] Measured gravimetrically by weighing dried membrane cakes.

In experiments with high $\bar{G}t_{mix}$ ($\bar{G}t_{mix} = 50{,}400$), medium $\bar{G}t_{mix}$ ($\bar{G}t_{mix} = 17{,}880$) and

low $\bar{G}t_{mix}$ ($\bar{G}t_{mix} = 1{,}890$), mixing rates were 40, 20, and 10 rpm while mixing

duration was 20, 20, and 6 min, respectively. The values of $\bar{G}$ were calculated using the

impeller diameter of 7.5 cm and the G values in these experiments were 42.0, 14.9,

and 5.3 s^{-1}, respectively. To calculate these values impeller constant for turbulent flow

(K_T=2.25) was used. This was justified based on the values of the impeller Reynolds

number, N_{Re}, for the three flocculation conditions tested ($N_{Re} \sim$ 4180, 2090, and

1050, respectively) and the fact that the dependence of K_T on N_{Re} reaches a plateau

for $N_{Re} > 100$ (Wang et al., 2008).
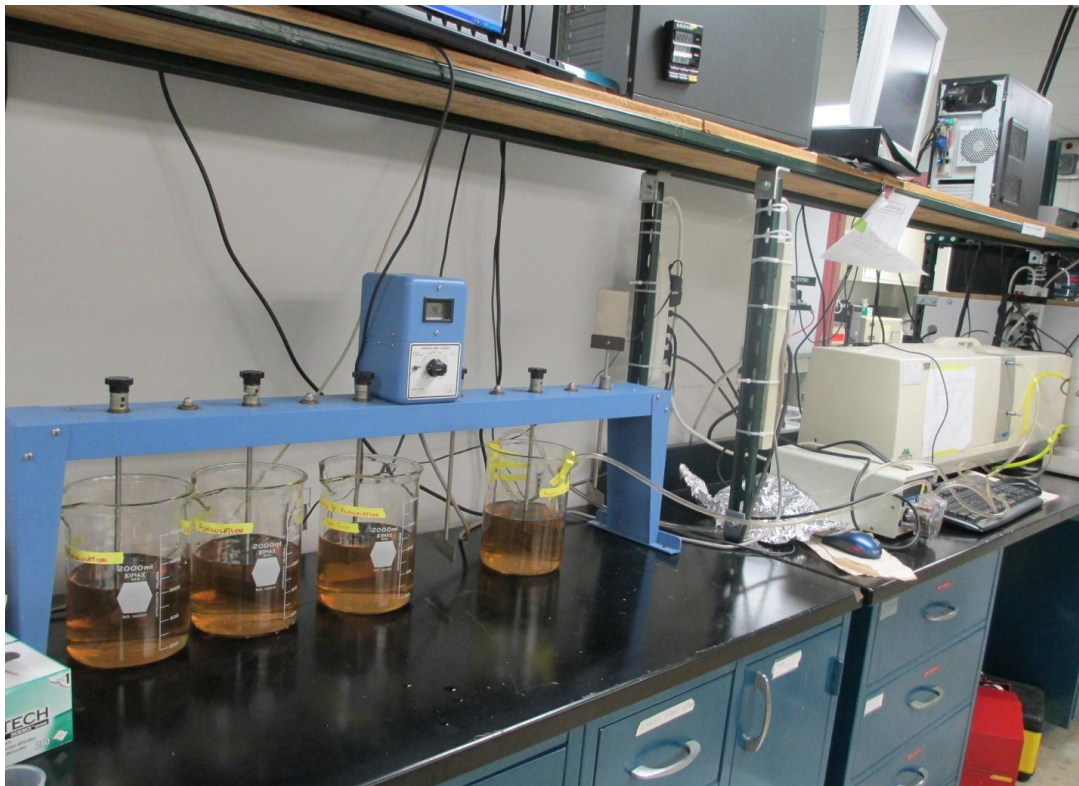
Figure 3-11: Floc formation study using Mastersizer

3.3.1.5 Light Scattering Technique

For humic acid flocs fractal dimensions were measured both by light scattering and box counting methods.

To measure the fractal dimension of flocs, a manufacturer-provided software module of the Malvern Mastersizer 2000 instrument was used to record the dependence of the intensity I of scattered light on the scattering vector Q:

$$Q = \frac{4\pi n}{\lambda} \sin\left(\frac{\phi}{2}\right), \tag{i}$$

where n is the refractive index of solvent, ϕ is the scattering angle, and λ is the wavelength of the incident light. The fractal dimension D_f of aggregates was determined from the linear fit to the double logarithmic plot of the dependence $I(Q) \propto Q^{-Df}$; this approach is valid when the aggregate is at least one order of magnitude larger than the size of the primary particles that form the aggregate (Lai et al., 1975; Wang et al., 2010). Highly branched and loosely arranged aggregates have low fractal dimensions, whereas tightly packed aggregates are characterized by high fractal dimension. Box counting procedure was same for clay and humic acid flocs.

3.3.2   Phase-II: Determining the effect of floc size and shape on membrane fouling, quality and quantity of permeate and flux decline.

3.3.2.1 Membrane Filtration

The same membrane filtration set up was used for humic acid floc suspension filtration as were utilized for clay floc suspension filtration. Here also two sets of membrane filtration experiments were performed. In one set of experiments the floc suspensions prepared on three $\overline{G}t_{mix}$ conditions were allowed to settle for 30 min and then transferred to pressurized feed reservoir for membrane filtration to model the conventional filtration treatment process Figure 3-2. In another set of experiments the floc suspensions were not allowed to settle after flocculation and they are directly transferred to pressurized feed reservoir for membrane filtration to model the direct filtration treatment process.
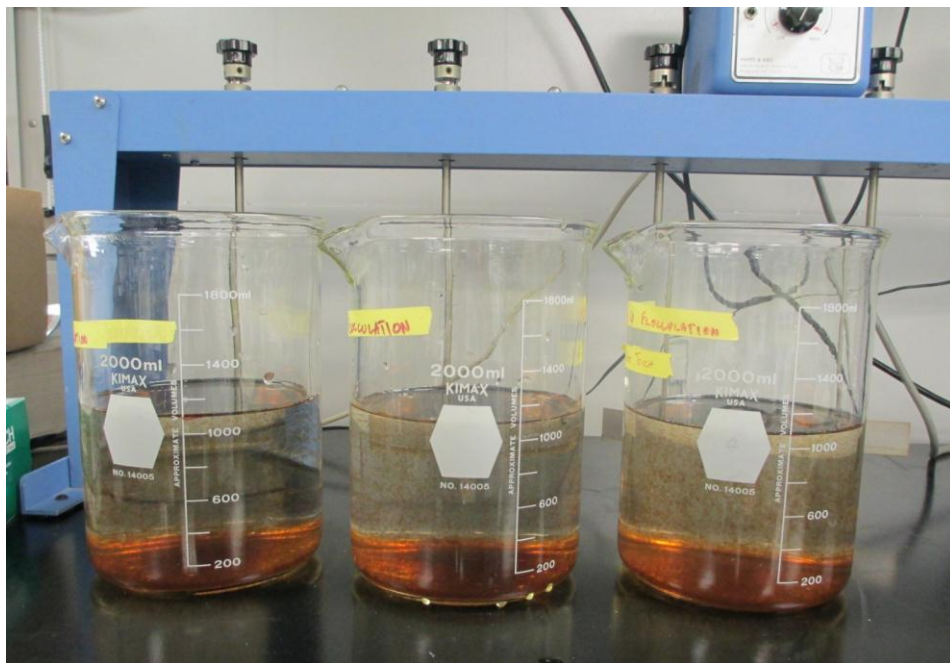
Figure 3-12: Humic acid flocs after 30 minutes of settling

RESULTS AND DISCUSSIONS

As already explained in chapter 3 that experimental work was divided into two sections and each section was further divided into two phases. The results and discussions chapter is also divided into two sections accordingly. Experiments with clay (Section A) will discuss the results of clay flocs coagulation/ flocculation and filtration and experiments with humic acid (Section B) will discuss the results of humic acid flocs coagulation/flocculation and filtration.

4.1 EXPARIMENTS WITH CLAY (SECTION A)

4.1.1   Coagulation and Dose Optimization

To determine the optimum alum dose for turbidity removal, coagulant dose optimization tests were performed under the synthetic feed water pH conditions (8.7 ± 0.1) (4.1). The results of turbidity removal of high turbidity synthetic feed water as a function of alum dose variations are shown in Figure 4-1. The turbidity of medium turbidity synthetic feed water was in a range of 30-35 NTU. Turbidity removal increased as the pH increased from 6.5 to 7.5 and decreased when pH is decreased by increasing alum dose. Maximum turbidity removal was achieved between the alum doses of 5.0-5.5 mg/L. Therefore the optimum alum coagulant dose for medium turbidity water was 5.5 mg/L. According to Amirtharajah and Mills (1982), adsorption and charge neutralization mechanisms are dominant coagulation for turbidity removal

under these conditions. Optimum alum coagulant dose was 3 mg/L at corresponding

pH of 7.5 ± 0.05 for low turbidity synthetic feed water (10-15 NTU).

Table 4-1: Experimental scheme for clay experiments

Experiment code	Feed water turbidity, NTU	Step 1: Coagulation		Step 2: Flocculation	Step 3: Settling
		Coagulant dosage, mg/L	pH	Mixing rate, rpm	Settling time, min
High$\bar{G}t_{mix}$→Settle	33.4 ± 1.2	5.5	7.5 ± 0.1	40	30 [a]
Low$\bar{G}t_{mix}$→Settle		6.5	5.5 ± 0.1	30	
High$\bar{G}t_{mix}$→Direct		5.5	7.5 ± 0.1	40	none [b]
Low$\bar{G}t_{mix}$→Direct		6.5	5.4 ± 0.2	30	
(High$\bar{G}t_{mix}$)LT→Settle	13.3 ± 1.0	3.0	7.5 ± 0.0	40	30 [a]
(High$\bar{G}t_{mix}$)LT→Direct		3.0	7.5 ± 0.1	40	none [b]

[a]Simulates conventional filtration process where the feed water was coagulated and subjected to settling prior to filtration
[b]Simulates direct filtration process where the feed water was coagulated but was not subject to settling prior to filtration
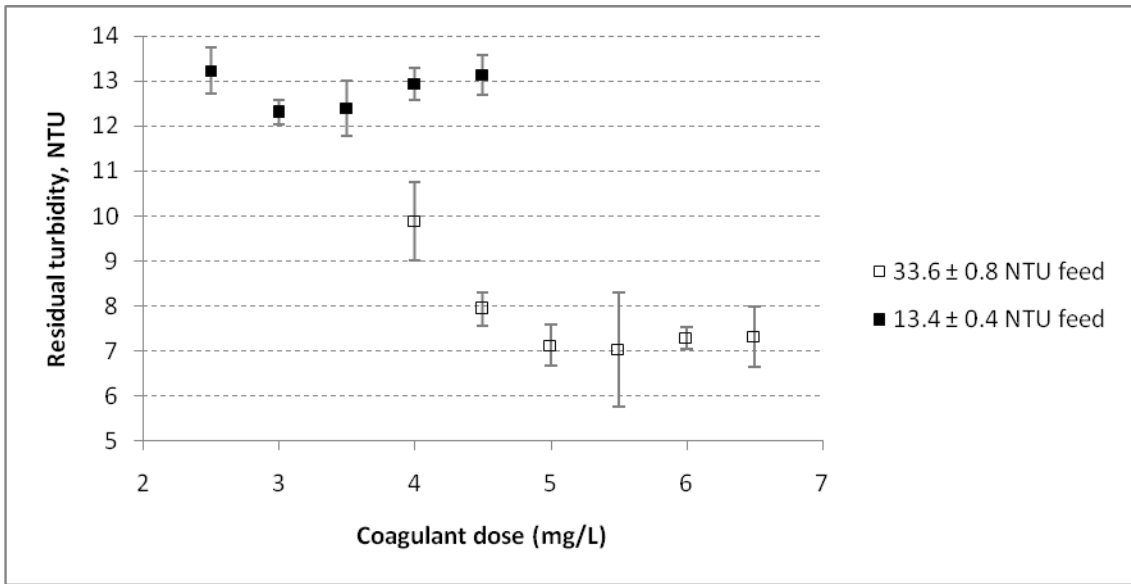
Figure 4-1: Turbidity removal as a function of coagulant dose.

4.1.2 Floc Size Distribution

Floc size distribution is one of the important parameter of floc growth that directly affects the removal of suspended colloids from the water and indirectly affects the membrane filtration efficiency. The volume average diameter of clay flocs in medium turbidity water (33 NTU), pH of 7.5 and alum coagulant dose of 5.5 mg/L is shown in Figure 4-2. In clay flocculation, flocs started to appear immediately and grow after 3 min of flocculation time and at the end of flocculation time, average floc size (d_{50}) reached to its maximum of 98.34 μm. According to the results of flocculation period, the highest percent volume of larger floc growth was achieved at 20 min of flocculation. As the flocs grow in flocculation process, aggregation and floc breakage occurs at the same time. In floc growth finally a steady-state arrives when the floc aggregation rate balances the floc breakage rate (Jarvis et al., 2005). The colloidal particles are found to aggregate very rapidly at the start of flocculation period due to

the effect of shear force. These aggregates have small inner pores. While cluster-cluster agglomeration in floc growth produces some small and compact clusters, under the strong shear conditions these clusters try to fit in the small inner pores of large aggregates. That was the reason flocs produced under high shear force conditions were stronger and compact in shape and show high fractal dimensions (Wang et al., 2011).
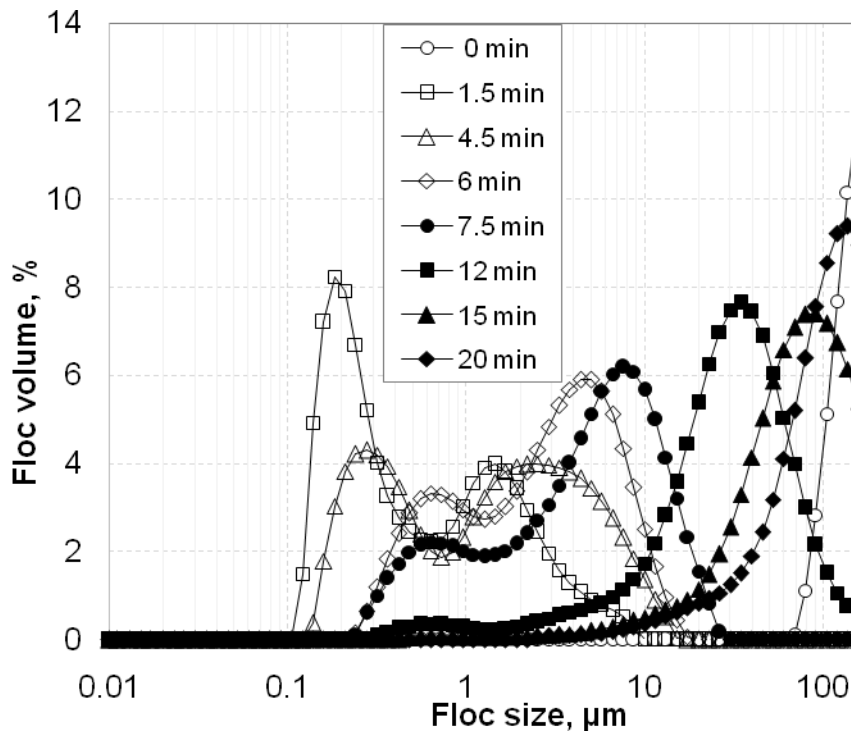
Figure 4-2: Clay floc size distribution as a function of flocculation time.

To measure the average diameter of flocs produced from low turbidity water (10-15 NTU), alum dose of 3 mg/L and pH of 7.5 their microscopic images were used. The reason was very less clay particles in this solution. Malvern Mastersizer is insensitive to such diluted solutions. To measure the accurate diameter of clay flocs using

microscopy images, was very challenging. The reason is the irregular shape of these flocs as they were not in true spherical shape. Flocs produced under low shear conditions were loose and branched and ultimately tend to break very easily (Waite, 1999).

4.1.3 Floc Images & Fractal Dimensions

The fractal dimension (D_f) values of clay flocs were obtained from their microscopy images. Box counting algorithm was applied to measure the D_f of flocs using their microscopy images. The D_f values of clay flocs measured by box counting are shown in Table 4-2.

Table 4-2: Structural characteristics of suspended clay flocs and membrane cakes as a function of coagulation/flocculation conditions.

Pretreatment conditions	Specific resistance of the membrane cake[a]	Fractal dimension	
	α_m, m/kg	D_{floc}[b]	D_{cake}
High$\overline{G}t_{mix}$→Settle	7.57±2.45	2.78±0.06	1.945±0.11
Low$\overline{G}t_{mix}$→Settle	4.73±1.77	1.74±0.14	1.919±0.20
High$\overline{G}t_{mix}$→Direct	4.16±1.65	2.87±0.01	1.902±0.13
Low$\overline{G}t_{mix}$→Direct	5.31±1.15	2.04±0.02	1.953±0.21
LT →Settle	8.94±2.63	2.71±0.01	1.943±0.11
LT →Direct	8.62±1.56	2.82±0.01	1.942±0.15

[a] computed for cake mass of 10mg
[b] fractal dimension of a floc's projection (determined using optical microscopy imaging of dried sample of the flocculated feed water)

Results showed that the D_f values of flocs produced at low Gt_{mix} conditions were lower than the flocs produced at high Gt_{mix} conditions. Which means more compact and stronger flocs were achieved under high shear conditions that promoted the floc breakup and restructuring (Jarvis et al., 2005) (Figure 4-3). It is inferred that loosely arranged and highly branched aggregates of low fractal dimensions were more prone to restructuring into tightly packed aggregates under conditions of high Gt_{mix}. Flocs produced from low turbidity (LT) water also showed the high fractal dimensions as they were flocculated on high Gt_{mix} conditions. Here the results showed that fractal dimensions of flocs depend highly on mixing conditions than the concentration of their respective solution.
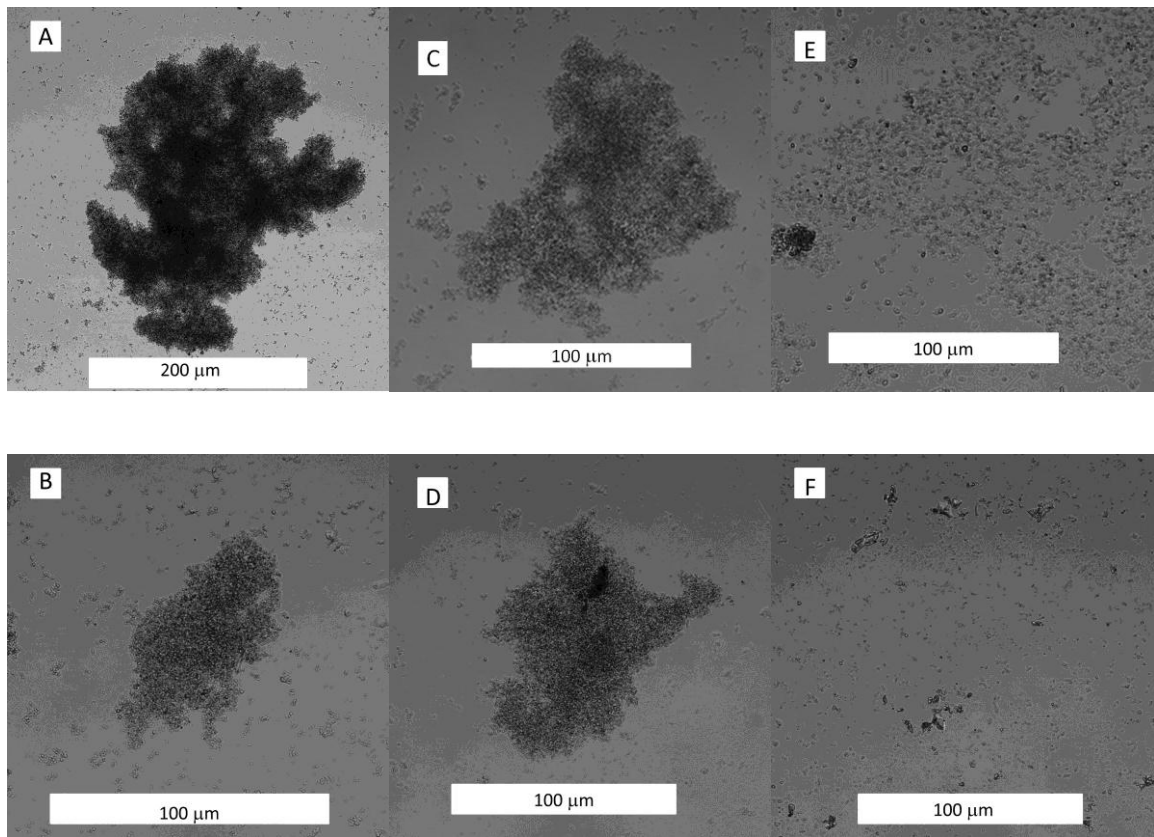
Figure 4-3: Confocal microscopy images of clay flocs formed under different conditions: (A) HighGtmix→Direct, (B) HighGtmix→Settle, (C) LT→Direct, (D) LT→Settle, (E) Low Gtmix→Direct, (F) LowGtmix→Settle

Results of fractal dimension measurements exhibited that there was no significant effect of pre-settling on flocs D_f. It was expected that flocs with different D_f values will settle at different settling rate.

4.1.4 Permeate Flux and Specific Cake Resistance α$_m$

Normalized permeate flux (*J*) and changes in specific cake resistance (α_m) during membrane filtration for different pretreatment conditions are shown in Figure 4-4. The reason for decrease in α_m with filtration time was the fractal growth (Wang et al.,

2010). In clay experimental conditions the cake compression was not significant (Figure 4-5).

Membrane filtration results illustrated the significant effect on the behavior of J and α_m. In direct filtration tests the normalized flux decline was higher and α_m was lower than the other set of experiments where the settling was applied before membrane filtration. Therefore, the conclusions were that in the absence of settling more thicker and porous membrane cakes were formed but because of the higher solid load on the membranes the overall hydraulic resistance was higher for these experiments.

A relatively different trend was observed in LT experiments. In LT→Direct filtration the permeate flux decline was less than the LT→Settle experiments. The reason for this high flux decline in LT→Settle experiments was the membrane cake formed by very small flocs. Such cake was very dense and packed therefore lead to higher permeate flux decline.
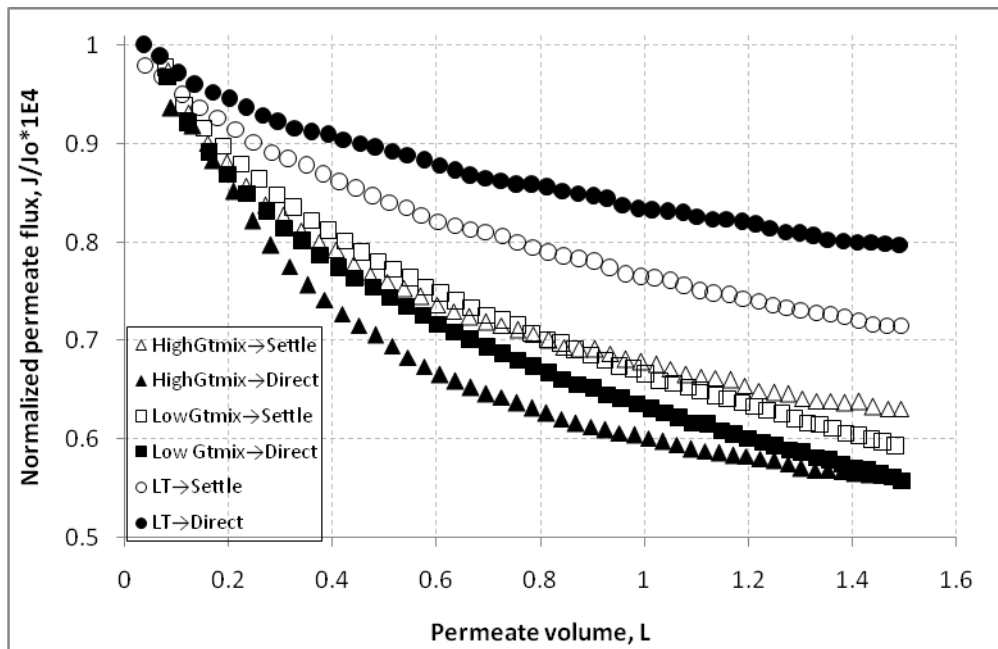
Figure 4-4: Permeate flux of the membrane cakes formed by ultrafiltration of clay flocs for different coagulation-flocculation conditions
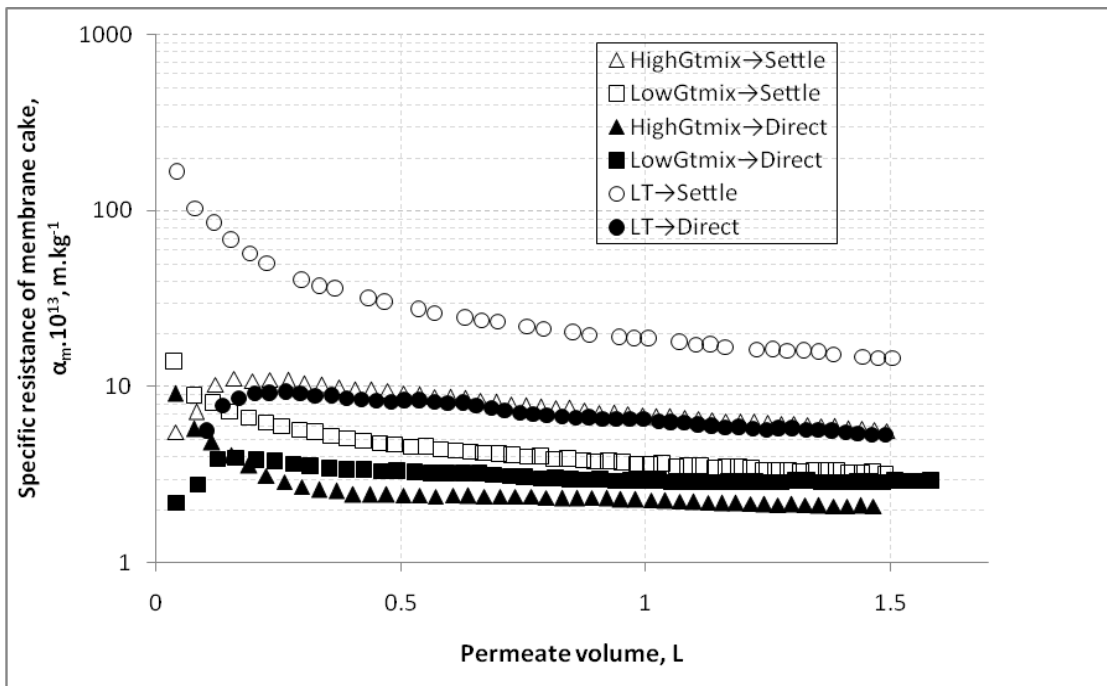
Figure 4-5: Specific hydraulic resistance of the membrane cakes formed by ultrafiltration of clay flocs for different coagulation-flocculation conditions.

4.1.5   Membrane Cake Fractal Structure

Changes in the membrane cake structure and membrane resistance were occurred with filtration time. A high quality ($R^2 \geq$ 0.999) scaling for membrane cakes of all conditions was achieved by applying the approach for clay flocs. As the increase in cake porosity with cake thickness has been reported before (Tarabara et al., 2004; Mendret et al., 2007; Mendret et al., 2009;), to our best knowledge our study is the first to report the evolution of cake porosity is subject to a scaling law.

The comparison between D_f of clay flocs and D_f of membrane cake showed that a broad range of D_{floc} values (1.74 $<D_{floc}<$ 2.87) gave a very narrow range of D_{cake} values (1.90 $<D_{cake}$ 1.95). The band of D_{cake} values squeezed near to 2, which was because of the breakup of flocs in the cake and cake restructuring.

4.2EXPERIMENTS WITH HUMIC ACID (SECTION B)

4.2.1   Coagulation and Flocculation

Optimum coagulant dose of alum was determined for maximum humic acid removal using humic acid synthetic solution by jar test apparatus followed by coagulation-flocculation and settling steps. The optimum coagulant dose for maximum humic acid removal was ranged between 70-80mg/L at 5.5 (Waite et al., 1999) (Fig 4.6).
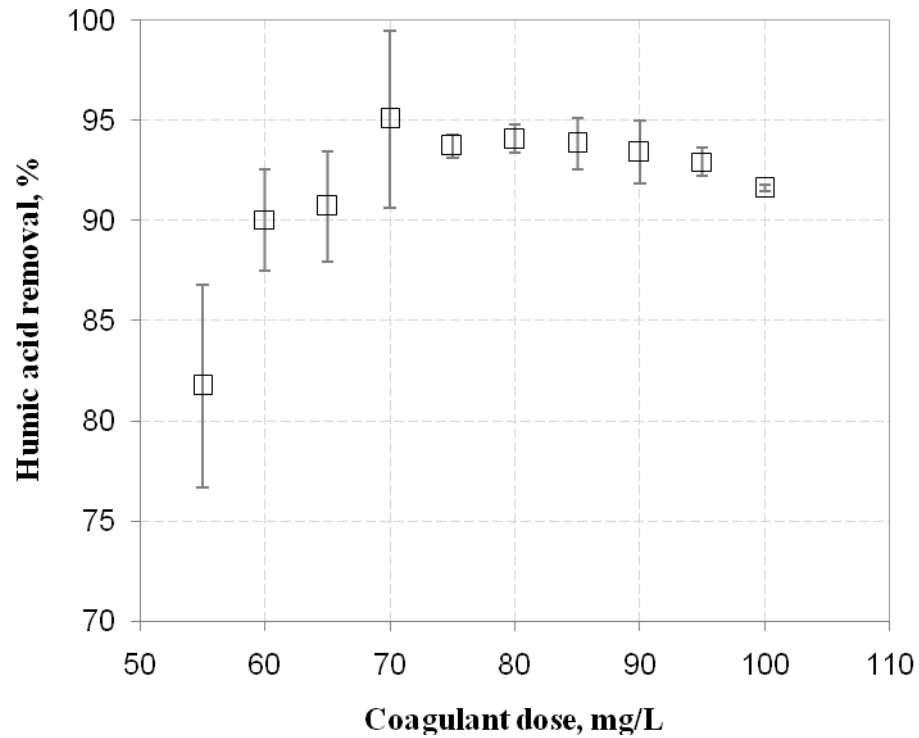
Figure 4-6: Humic acid removal as a function of alum dose.

The feed concentration of humic acid in diluted water was 14.1 to 16.7 mg(TOC)/L for optimum dose determination. For membrane filtration experiments the humic acid synthetic solution was further diluted to have a TOC content of 10mg/L in all experiments. So the corresponding humic acid content was 19.17mg/L in membrane feed (Waite et al., 1999). Here the optimum alum dose used was 70mg/L (i.e the lower bound in the optimal dose window of 70 to 80 mg/L, Figure 4-7). Therefore when alum coagulant dose was added to membrane feed the total solid contents of the feed was ~ 89.17 mg/L (i.e. 70 mg(alum)/L added to 19.7 mg(HA)/L).
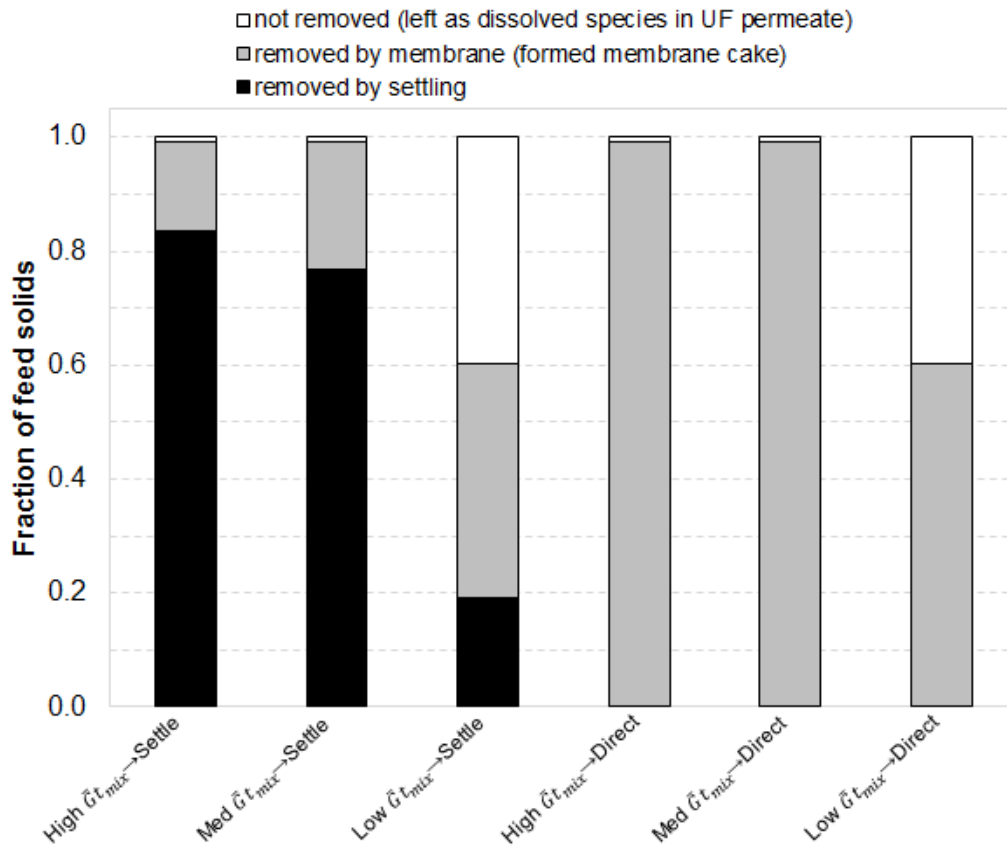
Figure 4-7: Fate of feed solids in the coagulation-flocculation-ultrafiltration process as a function of pretreatment conditions.

Figure 4-7 explains the fate of feed solids in the membrane filtration experiments. The mass balance on solids for membrane feed was developed in three steps:

1) The amount of solids removed by the membrane was calculated based on the initial total mass of feed solids and the cake mass measured by gravimetric analysis (89.17mg/L of feed suspension).

2) The dissolved species within the permeate stream that were not removed by membrane were calculated as initial feed solids (89.17 mg/L of feed

suspension) minus solids removed by the membrane. Step 1 was performed for direct filtration experiments so that removal of solids by settling in case of conventional filtration experiments could not be an issue. We also assumed that values determined by this approach can also be used for tests with settling because in principle settling should not affect the concentration of dissolved species.

3) In conventional filtration settling experiments, the amount of solids removed by settling was calculated as initial feed solids (89.17mg/L of feed suspension) minus solids removed by the membrane (calculated in step 1) minus solids not removed by membrane that were in dissolved form and pass with permeate stream (calculated in step 2).

In direct filtration experiments where no settling was provided, almost all the feed solids fouled the membrane and form a thick cake. According to the gravimetric analysis of the membrane cake (Table 4-3), in High$\bar{G}t_{mix}$→Direct and Med$\bar{G}t_{mix}$→Direct experiments 99.1% (=88.38/89.17*100%) of total solids initially present in the feed suspension deposited on the membrane surface. In experiments with Low$\bar{G}t_{mix}$→Direct conditions the fraction of feed solids removed by membrane was much lower because of an incomplete coagulation. In that case it can be assumed that dissolved alum was not rejected by 50 kDa membrane and did not contribute to fouling. A study by Wang et al., 2010 reported the residual Al in permeate in their experiments while they were working with a membrane of much larger pore size (0.22 μm). Another possible reason for lower cake mass in Low$\bar{G}t_{mix}$→Direct experiments

was the incomplete rejection of uncoagulated humic acid (MW 4 to 23 kDa) in these experiments. The TOC results measured for the permeate of High$\bar{G}t_{mix}$→Direct conditions showed the 100% humic acid rejection in these experimental conditions. These results indicated that under High$\bar{G}t_{mix}$→Direct conditions the coagulation was very effective in promoting humic acid aggregation and increasing its hydrodynamic size. This observation was confirmed by the TOC results of permeate in these tests that indicate the very less fraction of solids that left with permeate: 0.79/89.17*100% = 0.89%.

On the other hand, more effective coagulation in High$\bar{G}t_{mix}$→Direct conditions leaved a possibility of incomplete membrane rejection in other coagulation-flocculation conditions that were tested in current study. However, load on the membrane was much less in pre-settling conditions because pre-settling removed a large fraction of solids from the coagulated feed. More efficient removal of solids by flocculation was observed in High$\bar{G}t_{mix}$ conditions, while: 15.5% (=13.81/89.17*100%), 22.2% (=19.78/89.17*100%), and 41.0% (=36.56/89.17*100%) of feed solids deposited on the membrane surface under High$\bar{G}t_{mix}$→Settle, Med$\bar{G}t_{mix}$→Settle, and Low$\bar{G}t_{mix}$→Settle conditions, respectively.

4.2.2 Floc Size Distribution

Floc size is very important characteristic for water treatment as the removal of solids by settling and the performance of membrane filtration process downstream is highly dependent on floc size. The average diameter of suspended flocs as a function of time

prepared under high mixing ($\overline{G} \cong 42$ s-1) conditions, alum dose of 70mg/L and pH of 5.5 is presented in Fig 4.8. At the end of flocculation period that was 20 min, the maximum size of the aggregated floc was ~ 303 μm that was average of three replicate measurements. As the increase in floc size was function of flocs aggregation and breakup at the same time in flocculation. The steady state in flocs growth was a point achieved when flocs aggregation and breakup reached to equilibrium. In high mixing conditions the flocs growth steady state was achieved after ~ 10 min of flocculation when more than 99% of flocs that remained suspended were larger than 10 μm. Flocculation times of 1 min, 5 min, 7.5 min and 10 min generated the volume fraction of suspended flocs as 3.5%, 12.2%, 39.6% and 99.6%, respectively those were larger than 10 μm.
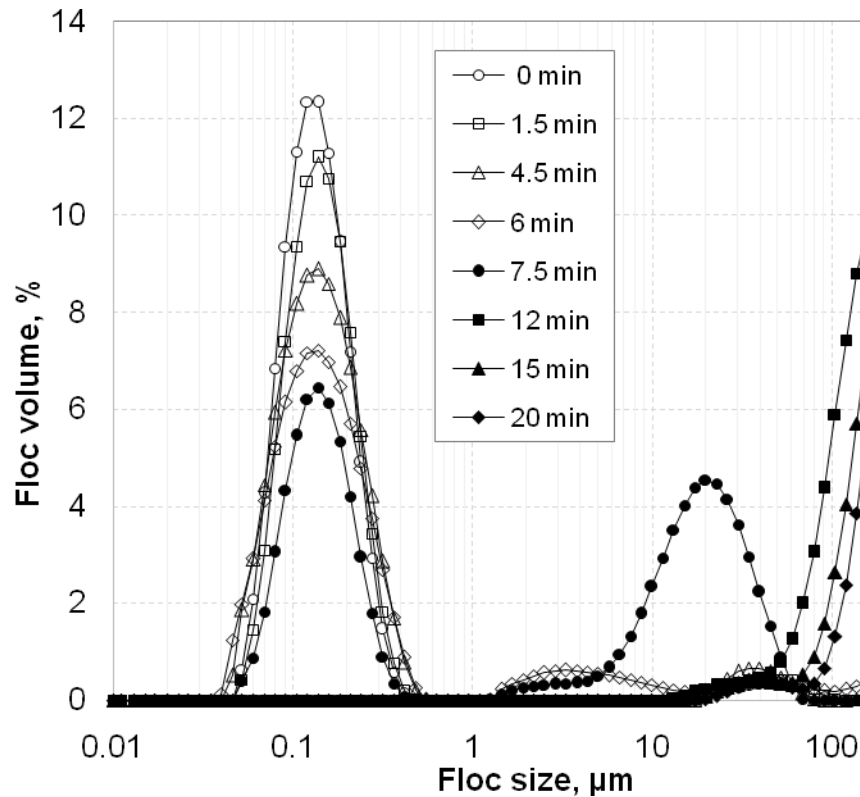
Figure 4-8: Floc size distribution as a function of flocculation time. Conditions: $\overline{G}$=42 s^{-1}; 70 mg(alum)/L; pH 5.5.

While the average diameter of flocs generated under medium mixing conditions ($\overline{G} \cong 15$ s-^{1}), was ~ 222 μm (Figure 4-9) at the end of 20 min flocculation period, at a pH of 4.8 and the same alum dose of 70 mg/L. At pH of 4.8, alum dose of 70 mg/L under slow mixing conditions ($\overline{G} \cong 5$s-^{1}) the flocs produced were very small in size. These flocs were referred as microflocs. Floc size measurement for these microflocs can be performed during the first 6 min of flocculation period only (Figure 4-9) and at that point light obscuration of mastersizer fell below the required threshold values by microflocs.
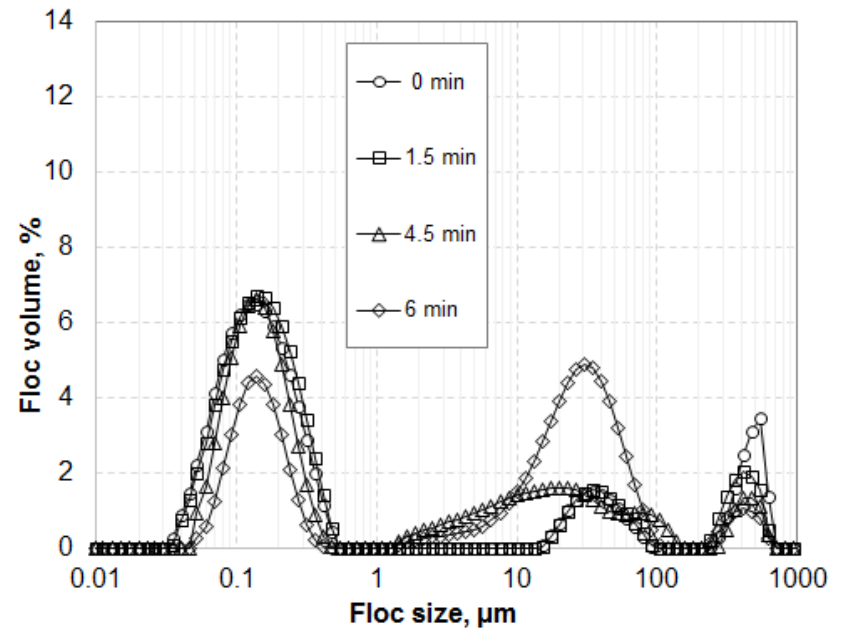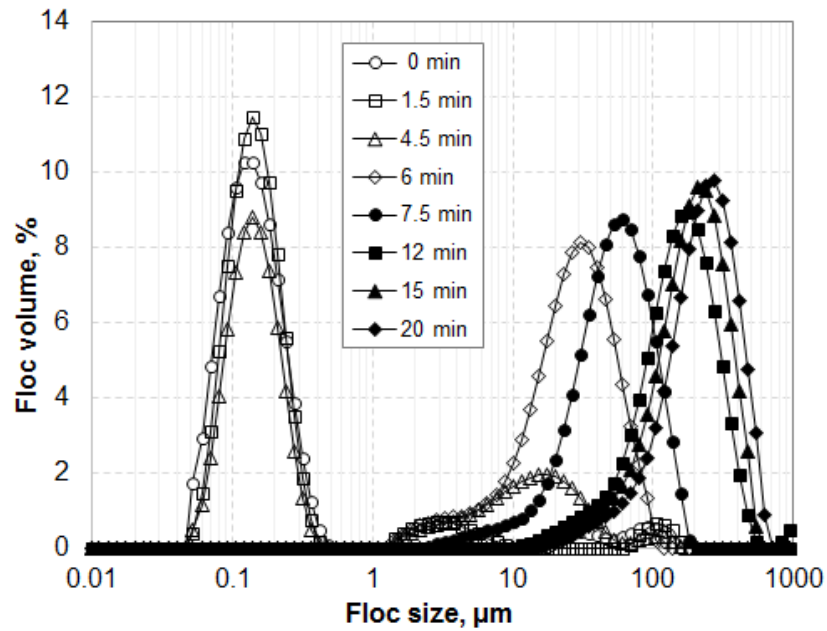
Figure 4-9: Floc size distribution as a function of flocculation time for different mixing conditions.

Left: $\bar{G}$=14.85 s⁻¹; 70 mg(alum)/L; pH 4.8

Right: $\bar{G}$=5.25 s⁻¹; 70 mg(alum)/L; pH 4.8
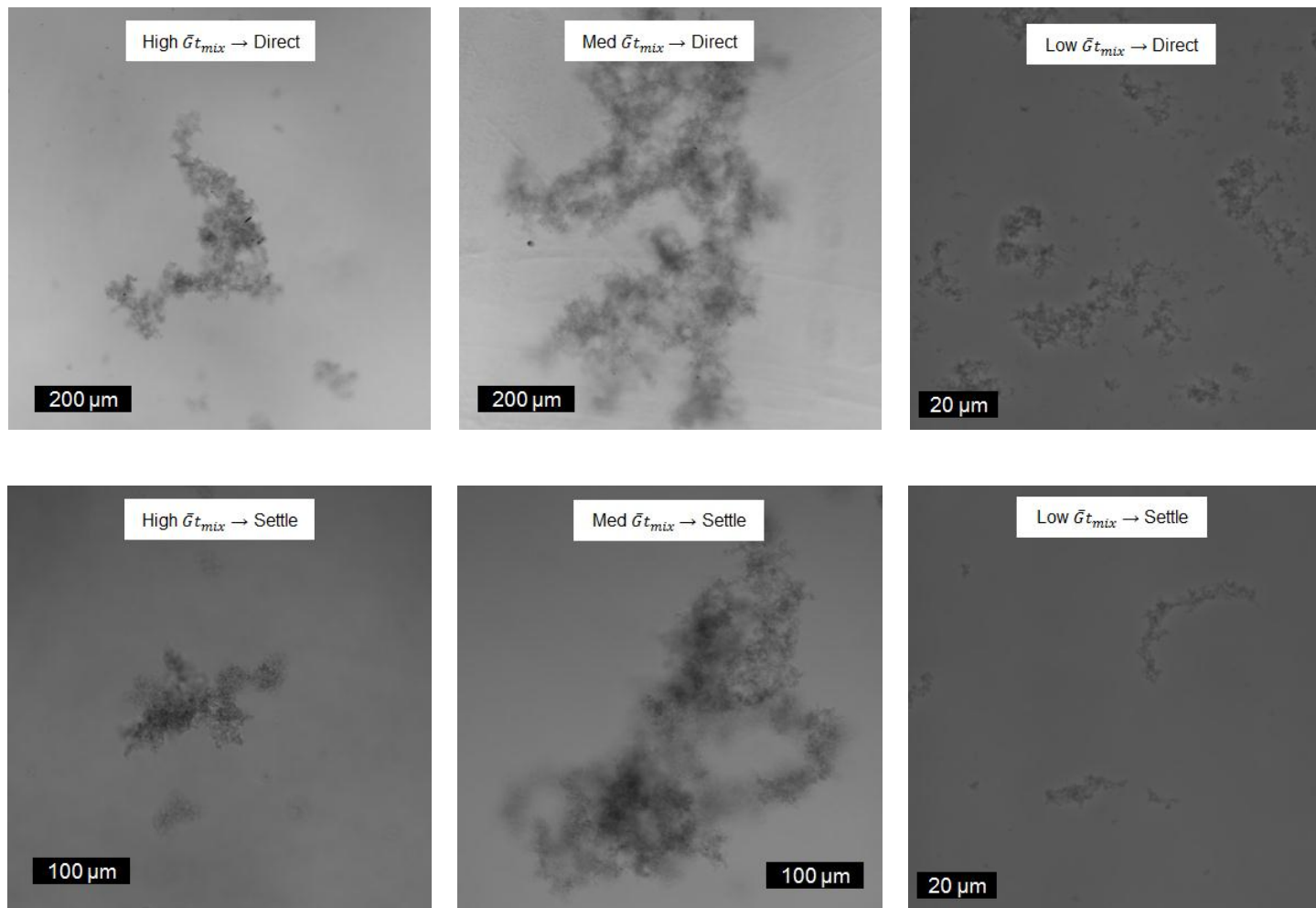
Figure 4-10: represents the direct comparison of sizes of typical flocs produced under three different pretreatment conditions by confocal microscopy images.

In experiments where Med $\overline{G}t_{mix}$ and High $\overline{G}t_{mix}$ conditions were practiced the flocs produced were more compact and large in size. Ultimately settling removed the larger and more compact flocs efficiently. The results were totally different in case of Low $\overline{G}t_{mix}$ conditions. In Low $\overline{G}t_{mix}$ conditions the mixing speed and flocculation time was not sufficient to produce compact and large enough flocs that can settle within 30 min of settling. Flocs produced at Low $\overline{G}t_{mix}$ conditions were only ~ 1μm in diameter that is at least an order of magnitude smaller than flocs generated at High $\overline{G}t_{mix}$ conditions. As the results indicated the higher fractal dimensions of non-settlable flocs (Figure 4-17), it was concluded that flocs produced under Low $\overline{G}t_{mix}$ conditions were not as much compact as the flocs generated under Med $\overline{G}t_{mix}$ and High $\overline{G}t_{mix}$ conditions.

4.2.3   Fractal Dimension D_f of Flocs

Fractal dimensions of flocs were measured using light scattering and confocal microscopy techniques. Table 4-3 presents the fractal dimension values of flocs obtained both by light scattering and confocal microscopy. To determine the fractal dimension of any aggregate using light scattering the Equation (i) (chapter 3) can only be used if the aggregate is at least one order of magnitude larger than the size of the primary particles that form it (Waite, 1999; Jarvis et al., 2005). Wang et al. (2010) reported humic acid diffusion coefficient of $2.46 \cdot 10^{-10}$ m^2/s for 8 mg/L aqueous solution of humic acid with the calcium concentration of 33 mg/L and pH 6 (Wang et al., 2001). This value gives the molecular diameter of ~ 1.7 nm according to the Stokes-Einstein equation. In our study primary particles were supposed to be of even

smaller size because the ionic strength of the solution was higher. Based on all these calculations the application of Equation (i) (chapter 3) to calculate the fractal dimension of humic acid flocs was justified.

Table 4-3: Characteristics of suspended flocs and of membrane cakes formed during ultrafiltration.

Experiment code	Characteristics of suspended flocs		Characteristics of membrane cakes		
	Fractal dimension [a], D_{floc}^{LS}	Fractal dimension [b], D_{floc}^{CM}	Fractal dimension [c], D_{cake}	Specific resistance [d], $\alpha_m \cdot 10^{13}$, m/kg	Specific resistance [e], $\alpha_m \cdot 10^{13}$, m/kg
High$\bar{G}t_{mix}$→Settle	2.42 ± 0.06	2.67 ± 0.02	2.968 ± 0.006	11.91 ± 0.57	9.29 ± 1.60
High$\bar{G}t_{mix}$→Direct	2.56 ± 0.03	2.72 ± 0.02	2.973 ± 0.011	5.10 ± 0.62	3.10 ± 0.54
Med$\bar{G}t_{mix}$→Settle	2.53 ± 0.03	2.71 ± 0.03	2.987 ± 0.005	9.80 ± 0.84	7.96 ± 0.98
Med$\bar{G}t_{mix}$→Direct	2.46 ± 0.05	2.73 ± 0.05	2.977 ± 0.003	4.61 ± 0.39	3.17 ± 0.12
Low$\bar{G}t_{mix}$→Settle	2.06 ± 0.05	2.16 ± 0.14	2.943 ± 0.007	6.79 ± 0.39	3.37 ± 0.33
Low$\bar{G}t_{mix}$→Direct	1.95 ± 0.02	2.12 ± 0.03	2.931 ± 0.001	5.93 ± 0.51	3.17 ± 0.26

[a]Determined by light scattering.
[b]Determined by confocal microscopy imaging and the box counting method.
[c] Reported with a higher accuracy to illustrate statistically significant differences in D_{cake} for different pretreatment conditions.
[d]Measured at the time that corresponds to the cake mass of 10mg.
[e]Measured at the end of each experiment (i.e. for permeate volume of 1.5 L)

The fractal dimension values obtained from two different techniques gave different results. The values of fractal dimensions measured in light scattering experiments were somewhat lower than the values obtained from confocal microscopy images by applying the box counting algorithm for the same flocs. The difference in these two values can be explained as resulting from floc breakup in slide preparation steps. In confocal microscopy, images of flocs on the slides were prepared for flocs produced in different experimental conditions. So the chances of floc breakage were higher during sampling and sample transfer of flocs from flocculation jar to microscopic glass slide. This was quite certain that floc breakup and restructuring lead to denser flocs with higher fractal dimension (Figure 4-11).
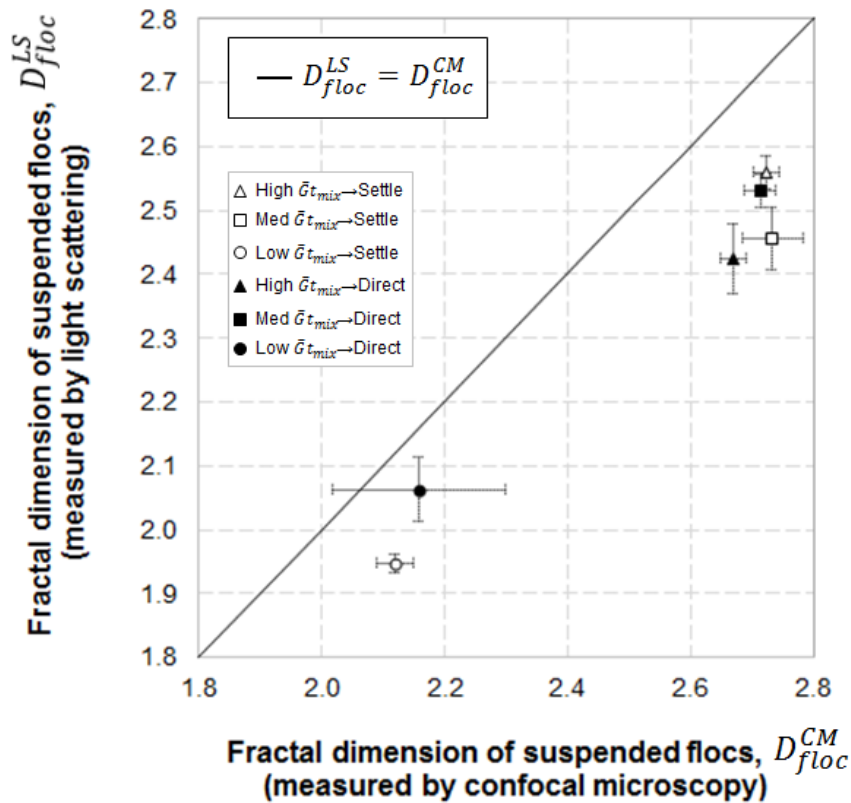
Figure 4-11: Effect of pretreatment conditions on suspended flocs' fractal dimension measured by two methods.

Flocs produced under medium and higher Gt_{mix} conditions were more compact and had higher fractal dimensions indicating the experimental conditions that promote flocs breakup and restructuring. However, the flocs produced at low Gt_{mix} conditions were highly branched and loosely arranged structures having lower fractal dimension values as compared to other two Gt_{mix} conditions. So these highly branched flocs can break up and restructure in more compact and strong flocs under high Gt_{mix} conditions.

The fractal dimension results did not indicate any significant statistical difference between settleable and non-settleable flocs for all three mixing conditions. It was supposed that flocs

with higher fractal dimensions would settle on a different settling rate (Veerapaneni and Wiesner, 1996; Li and Logan, 2001).

4.2.4   Ultrafiltration

The variations in permeate flux decline during ultrafiltration of pre-coagulated feed suspensions prepared under different Gt_{mix} and pH conditions is presented in Figure 4-12. The normalized permeate flux decline was higher for direct filtration experiments as compared to the other set of experiments where the settling was provided to pre-coagulated feed suspension prior to ultrafiltration. For direct filtration experiments the lowest normalized permeate flux decline was observed for low Gt_{mix} conditions where the solid load was less on membrane. The reason behind this was the inefficient coagulation under these mixing conditions which ultimately lead to the passage of un-coagulated humic acid particles and also the free Al from the membrane pores.
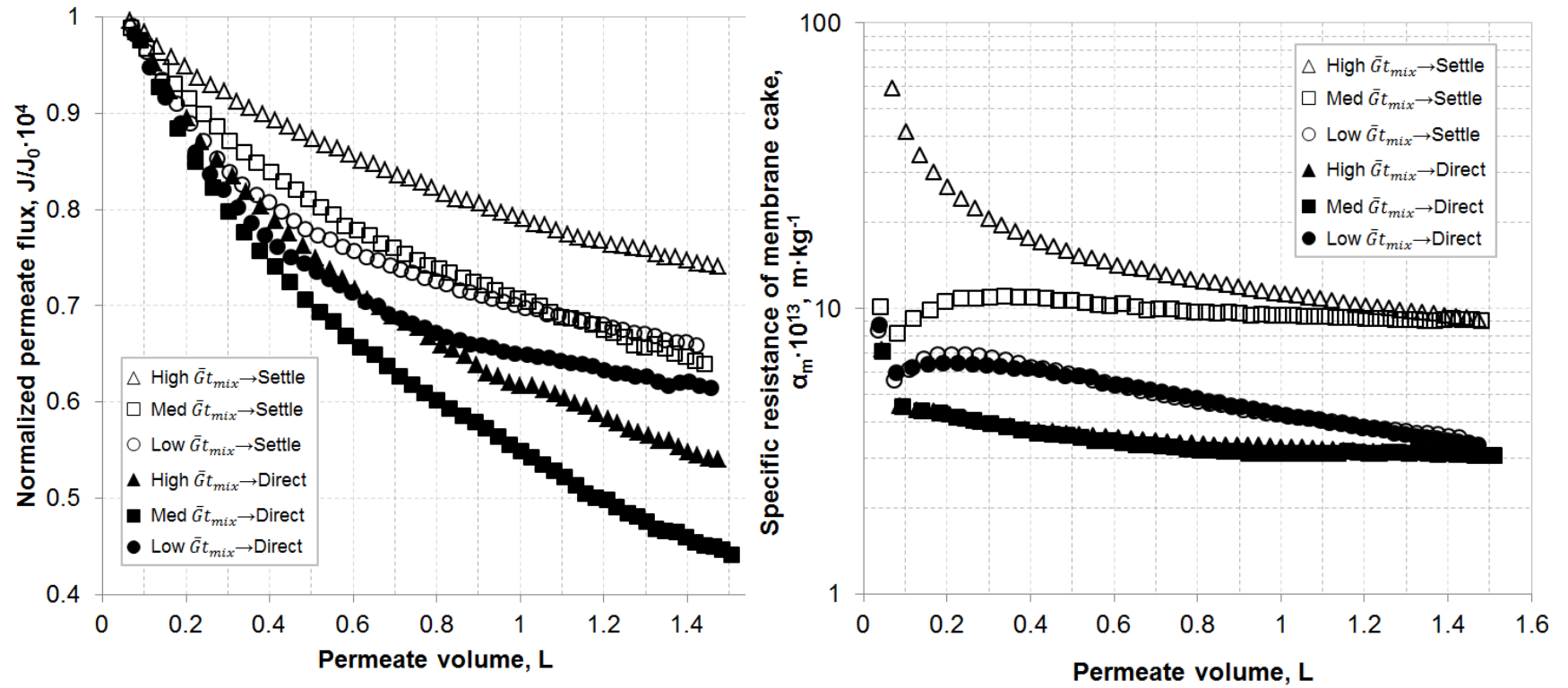
Figure 4-22: Transient behavior of permeate flux (left) and specific hydraulic resistance (right) of the membrane cake formed by humic acid flocs for different pretreatment conditions.

However, the lowest normalized permeate flux decline was observed for High$\overline{G}t_{mix}$→Settle conditions where the overall load on the membrane was very less. The explanation for this less normalized permeate flux decline is that flocs produced under High$\overline{G}t_{mix}$ conditions were very compact and large in size. So the 30 min settling played a very vital role in these experiments with removing a major part of solids suspension and leaving behind a very less amount of solids in the membrane feed for ultrafiltration. These conditions ultimately lead to fewer declines in membrane flux.
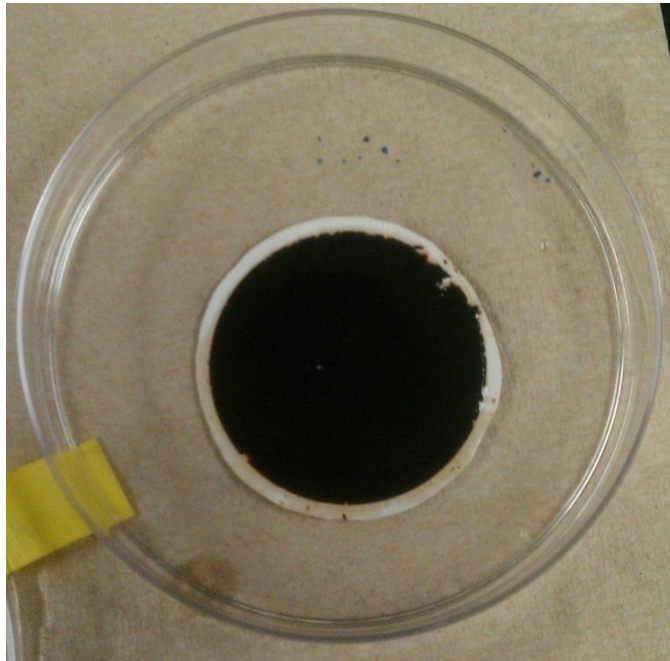
Figure 4-13: Humic acid cake deposition on membrane.

Figure 4-12 is showing the changes in specific cake resistance during ultrafiltration for different pretreatment scenarios. An overall decrease in α_m was observed with the filtration time which was an indication of fractal growth. Lee et al. (2005) reported the

cake compression in their membrane filtration experiments which was inconsistent to our results (Lee et al., 2005). In our study the experimental conditions did not support the cake compression significantly so that it can outweigh the porosity increase characteristic for a growing fractal deposit (Figure 4-12).

Due to the difference in mass of membrane feed suspension for various pretreatment experimental conditions, the difference in transient behavior of permeate flux and specific cake resistance was observed. For pretreatment conditions the settling was having the most major effect on ultrafiltration results and cake formation. The permeate flux decline was higher for direct filtration tests indicating a decrease in specific cake resistance values. The results were just opposite of that of conventional filtration tests where settling was provided prior to ultrafiltration. Thus, the overall conclusion for ultrafiltration tests and cake formation was that under direct filtration conditions the membrane cakes formed were more porous and thicker in nature as compared to the cakes formed under conventional filtration conditions. The reason why these cakes showed the higher hydraulic resistance was that despite high permeability of these cakes, the overall deposited mass on membrane was higher in direct filtration experiments.

Changes in cake porosity as the thickness of cake increases on the membrane surface, has been illustrated in Figure 4-14. Cake porosity is highly dependent on the diameter of the cake forming particles. In our study, the primary particle size (d_c) was estimated by hydrodynamic diameter of humic acid colloids in its stock solution before coagulation and was measured by dynamic light scattering at $\lambda = 254$ nm (Dulebohnet

et al., 2014). The particle size measurements were also carried out using Mastersizer 2000 and the values achieved were, to some extent, smaller than expected but had the same order of magnitude (Figure 4-8). As the Mastersizer is generally suitable to measure the size distribution range of polydisperse suspensions, in our study we decided to use the results of dynamic light scattering test for size estimation since it gave the more accurate results for very small particles particularly those are in submicron range in the suspension.
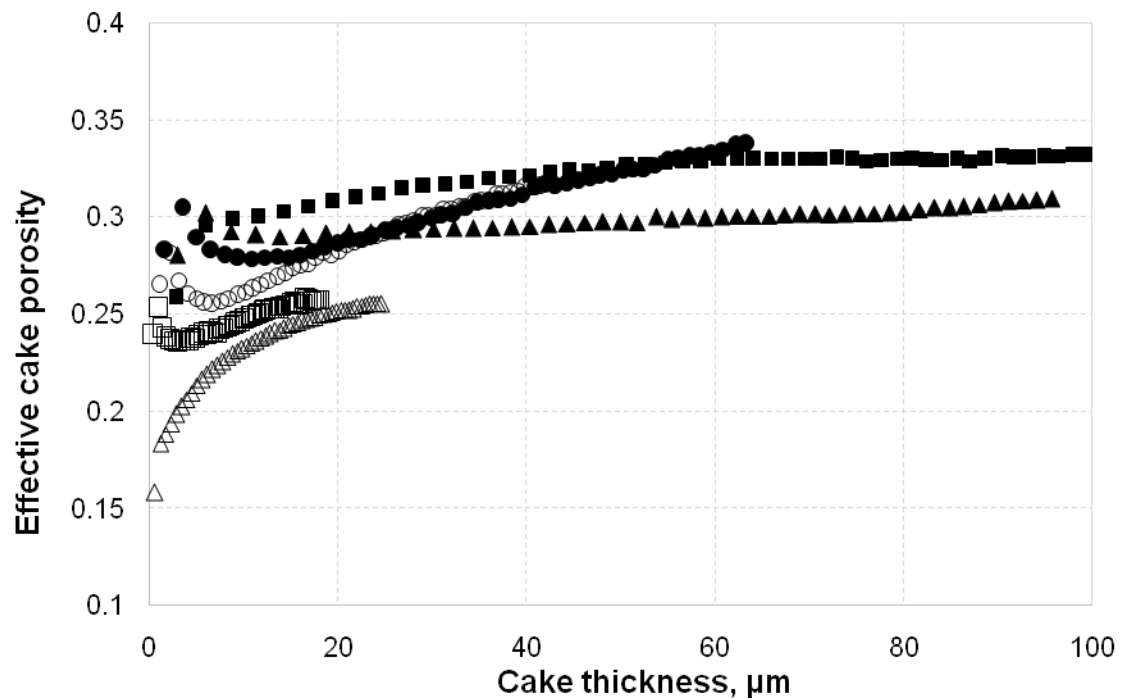
Figure 4-14: Evolution of average cake porosity (based on measured permeate flux and the Happel model) during cake growth for different pretreatment scenarios.

The primary humic acid particles were assumed to be spherical in shape ($K_K = 5$; $\psi = 1$) with a density of 1.5 g/cm^3. Typical organic-rich soils have the same density values (MacFarlane, 1969).

In principle, porosity of the cake can be observed in three different forms: porosity of primary particles, intra-aggregate porosity (i.e. porosity of those aggregates that make up the cake), and inter-aggregate porosity (i.e. porosity that is because of the space between aggregates that make up the cake). In humic acid experiments the hydrodynamic size of humic acid colloids was ~ 0.25 μm and the humic acid-alum aggregates were several microns in size (~ 307 μm in High$\overline{G}t_{mix}$conditions). Park et al. (2006) observed and compared the contributions of inter-aggregate porosity and intra-aggregate porosity in cake formation separately. Values of average porosity (averaged over the entire volume of cake) for humic acid-alum cake are reported in Figure 4-14 that includes both intra-and inter-floc porosity. In our study the porosity calculations were based on the assumption that primary particles were impermeable. When the primary particles in membrane filtration are not impermeable, the flow through particles needs to be considered (Veerapaneni andWiesner, 1996). In such cases Brinkman or Happel equations should be used to calculate the porosity instead of the Carman-Kozeny equation (Li and Logan, 2001).

As the cake thickness increased the average porosity also increased in almost all membrane filtration experiments except for some experiment in the very early stages of filtration where the random close packing value approached 0.36. In this study, we

predicted the increase in cake porosity numerically (e.g. Harmant andAimar, 1998) as the cake thickness increased and that was confirmed experimentally by invasive (e.g. Meeten, 1993;Tarabara et al., 2004) and non-invasive (e.g. Pignon et al., 2003; Mendret et al., 2009; Mendret et al 2007; Pignon et al., 2004) assessment of membrane cake structure.

4.2.5   Fractal Structure of Membrane Cake

Membrane filtration results showed that mechanism of membrane fouling was cake filtration while working with humic acid feed water. However, change in filtration time lead a change in cake resistance. A high quality ($R^2 \geq 0.9995$) scaling was observed for all experimental conditions by applying the approach from Chapter 2 (approach for humic acid flocs). Such scaling is explained in Figure 4-15. The power law dependence in terms of the mass and thickness of the membrane cake can be explained by using Equation. (2, chapter 2). As previous studies (Mendret et al., 2009; Mendret et al., 2007; Tarabara et al., 2004) have already reported that cake porosity increased with cake thickness, our study reports that the growth of cake porosity is subjected to a scaling law (Equation. (2 & 3b, chapter 2) and Figure 4-15).
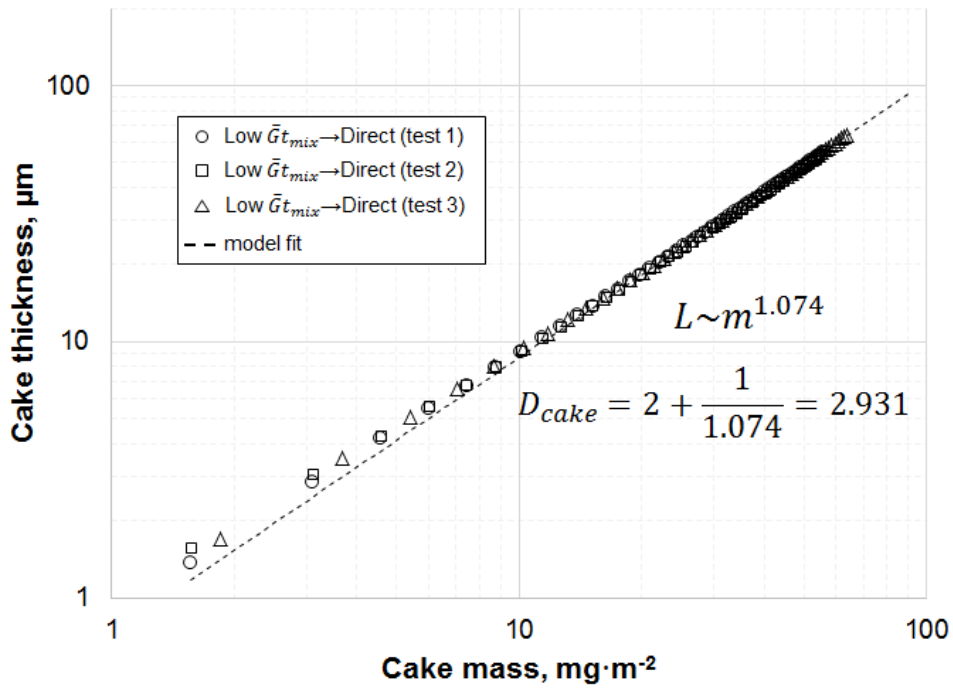
Figure 4-15: Illustration of the observed scaling indicative of the fractal structure of membrane cakes. Scaling is shown for only one of six pretreatment conditions.

Ultrafiltration results of most of the experiments illustrated the scaling throughout the entire duration of filtration. Only in a few experiments during the early stages of ultrafiltration (e.g. for $Low\overline{G}t_{mix} \rightarrow Direct$, Figure 4-15), the results deviated from this behavior. For all experiments the curve fitting was performed by picking the portion of the flux data that was obtained from later stage of ultrafiltration and growing the data set point by point until the square of the Pearson product moment correlation coefficient (R^2) decreased below 0.9995. As a result, every fractal dimension value reported in Table 4-3 and Figure 4-16 was achieved by the largest

possible dataset that still affords a high quality ($R^2 \geq 0.9995$) linear fit on a double log graph.
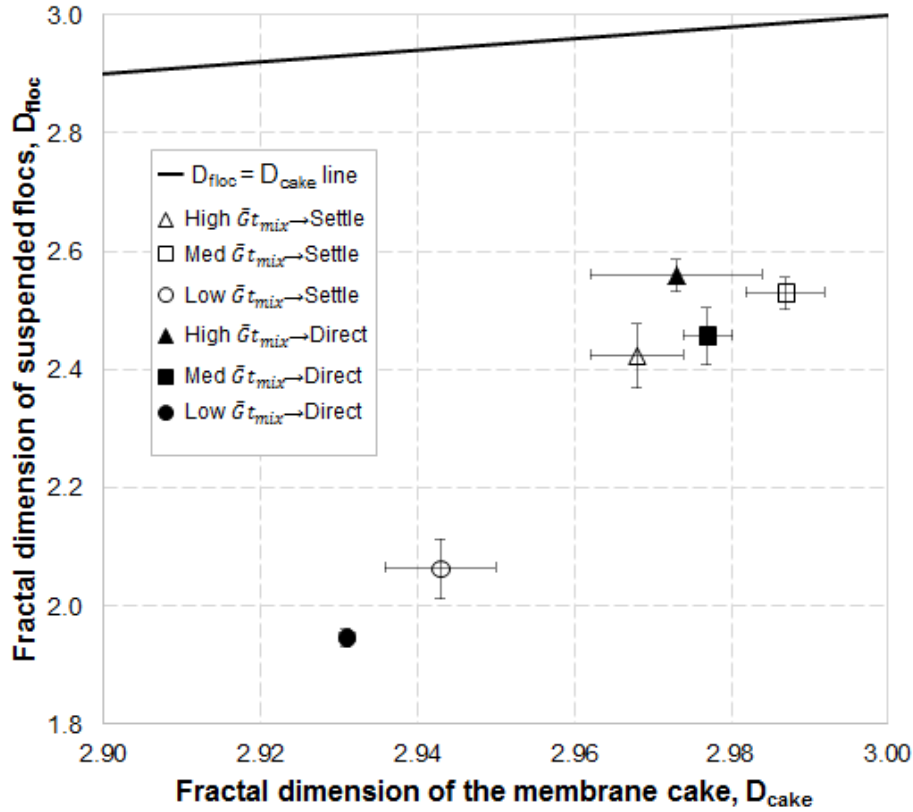
Figure 4-16: Relationship between the fractal dimension of suspended flocs, and the fractal dimension of membrane cakes, formed from these flocs as a function of pretreatment conditions. D_{floc} values used in this figure were measured by light scattering.

A number of observations were extracted by the comparison of fractal dimension of suspended flocs and fractal dimension of membrane cakes (Figure 4-16):

a) The correlation of fractal dimension of suspended flocs and fractal dimension of membrane cake was found to be weak ($R^2 = 0.86$). In consistence with observations of Antelmi et al. (2001), this correlation indicates that "memory"

of the aggregate structure was partly retained during the formation of membrane cakes from particle aggregates.

b) Flocs formed with lower fractal dimension values under the conditions of low$\bar{G}t_{mix}$produced the membrane cakes with lower fractal dimension as compared to the flocs formed under conditions of medium and high $\bar{G}t_{mix}$.

c) Pre-settling had not a significant effect on the correlation of fractal dimension of suspended flocs and fractal dimension of membrane cakes. In other words, difference between settlable and non-settlable flocs was not imperative.

d) The most important observation of the relationship between fractal dimension of suspended flocs and fractal dimension of membrane cake was that a broad range of D_{floc} values from 1.95 to 2.56 (resultant to different pretreatment conditions) ended up into a narrow range of D_{cake} values (from 2.92 to 2.99) representing the importance of humic acid flocs breakup and restructuring as they fitted into a growing cake.

As the cake permeability (Figure 4-12, right) and porosity (Figure 4-14) tends to increase with the filtration time, most of the breakup and restructuring of flocs occured at the time of their addition to the cake. These results found out in our study were in appropriation with the findings of Antelmi et al who used SANS for membrane cake characterization and reported very low fractal dimensions for the pore space in the membrane cakes (Antelmi et al., 2001).

4.2.6 Floc structure as the link between pretreatment conditions and ultrafiltration flux

In this study mass-based specific cake resistance, α_m, given by eq. (xx) was used to compare permeability values from different experiments. The relationship between α_m (a metric of flux performance) and fractal dimension of suspended flocs, D_{floc} (a metric of floc microstructure) and the effect of pretreatment on them are illustrated in Figure 4-17. The values reported in the Figure 4-17 are the one that translates the end of ultrafiltration experiments which means when 1.5L volume of filtrate was collected.
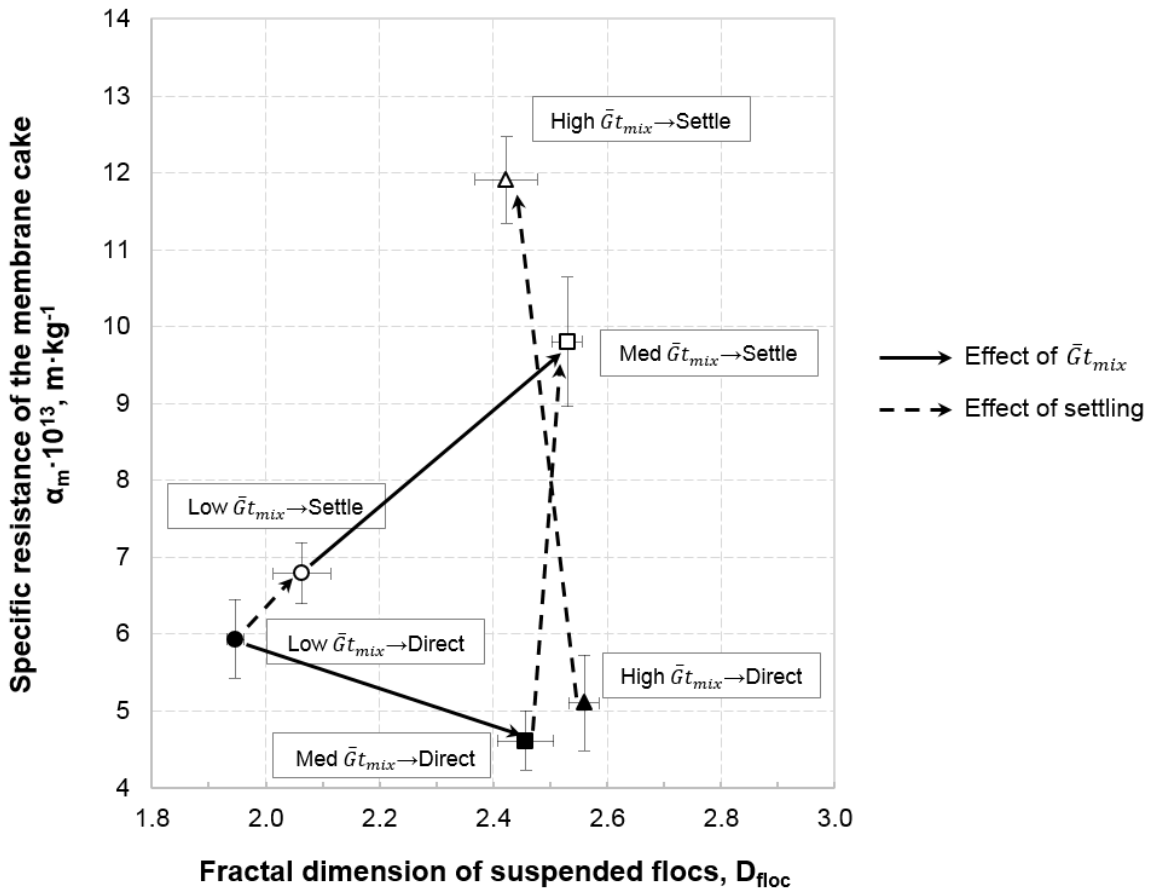
Figure 4-17: Effect of pretreatment on the structure and permeability of membrane cakes. Effect of mixing during flocculation and settling are illustrated by dashed and solid arrows, respectively.

4.2.7 Effect of $\bar{G}t_{mix}$

In consistence with increase in $\bar{G}t_{mix}$ (○→□) the specific cake resistance tends to increase in filtration tests with pre-settling. This was an expected result when we had more open floc structure (as reflected by lower values of D_{floc} and D_{cake}, seeTable4-3, Figure 4-16) and, most likely, the flocs produced under conditions of lower $\bar{G}t_{mix}$ packed into membrane cakes of higher permeability. In contrast to filtration with pre-settling, an opposite trend was observed in direct filtration (●→■, ●→▲) where membrane cakes of larger specific resistance were achieved with pretreatment at low$\bar{G}t_{mix}$(-●-). This different trend can be streamlined by assuming that in Med$\bar{G}t_{mix}$→Direct (-■-) and High$\bar{G}t_{mix}$→Direct (-▲-) tests more porous cakes were formed by very large flocs in the settlable fraction even when restructured. Data achieved from Low$\bar{G}t_{mix}$→Direct (-●-) and Low$\bar{G}t_{mix}$→Settle (-○-) experiments also supported this explanation. The difference in feed water floc populations in these two tests was not significant with both consisting of the small flocs; in consistence with this data, the values of D_{floc} and α_m differ only slightly between these two sets of pretreatment conditions. The results of α_m andD_{floc} for High$\bar{G}t_{mix}$ conditions were in consistence to Med$\bar{G}t_{mix}$ results.

It's the common trend in coagulation and flocculation that the suspended particles when they destabilized and form aggregates, these aggregates packed into more porous cakes and ultimately translated into lower specific hydraulic resistance, α_m. The results

obtained in this study showed that although aggregates breakup and restructure in cake formation ($D_{cake} > D_{floc}$), but still some "memory" of the aggregate structure was preserved during the formation of cake. In our study the data received from filtration tests without pre-settling (i.e. Low$\overline{G}t_{mix}$→Direct, Med$\overline{G}t_{mix}$→Direct, and High$\overline{G}t_{mix}$→Direct) showed that suspended flocs of higher fractal dimension were produced under High$\overline{G}t_{mix}$→Direct and Med$\overline{G}t_{mix}$→Direct conditions. The specific cake resistance (Figure 4-17) of membrane cakes evolved from these flocs was statistically same (in case of High$\overline{G}t_{mix}$→Direct) or slightly lower (in case of Med$\overline{G}t_{mix}$→Direct) when we compare them to the membrane cakes formed by Low$\overline{G}t_{mix}$→Direct tests. The possible reason for this trend can be the smaller size of suspended flocs produced under Low$\overline{G}t_{mix}$→Direct conditions (Figure 4-10). This explained that both floc size and fractal dimension affect filterability of cake (Lee et al., 2005; Waite et al., 1999).

4.2.8 Effect of Pre-settling

When we observed the effect of settling on cake structure and permeability, it was same for all coagulation-flocculation conditions: in all cases when the membrane cakes were evolved by removing the settlable portion of suspended flocs by pre-settling, they illustrated the higher specific cake resistance. For flocculation conditions of medium

and high $\overline{G}t_{mix}$ (▲→△, ■→□) the effect of settling on α_m was much more prominent that for low $\overline{G}t_{mix}$ (●→○). This can be attributed to a larger difference between settlable and non-settlable flocs in fully flocculated water. Remarkably, the denser cakes were evolved when pre-settling was applied prior to filtration, the change was only in α_m but not in D_{cake}.

4.2.9 Implications for Water Treatment Practice

However, a model feed water matrix of humic acid was used in this study but still the findings and conclusions of this study can be applied for the filtration of high organic content surface water. In our study the lowest flux decline was found for High$\overline{G}t_{mix}$→Settle pretreatment (-△-, Figure 4-12) in experiments where full pretreatment (coagulation + flocculation + settling) was applied. In this case the cake evolved was the thinnest as only a small fraction of solids (15.5%; Figure 4-8, section 4.1) deposited on the membrane surface and this thinnest cake gave the highest specific resistance (α_m= 9.29·10^{13} m/kg, Table 4-3). The reason of this highest specific resistance was that the very less porous cakes evolved by non-settlable flocs which were very small in size. Membrane cakes of lower fractal dimension (D_{cake}=2.94, Table 4-3) and relatively low specific hydraulic resistance (α_m= 3.37·1013 m/kg, Table 4-3) were produced under Low$\overline{G}t_{mix}$→Settle pretreatment

conditions because of the fact that here incomplete flocculation produced open

structure (Figure 4-10) and low fractal dimension (D_{floc}^{CM}=2.16, Table 4-3) flocs.

However, because of the larger solids load (41%, Figure 4-8) on the membrane, the

flux decline (-○-, Figure 4-12) was higher than in the case of High$\overline{G}t_{mix}$→Settle

pretreatment. As far as the above considerations are concerned, High$\overline{G}t_{mix}$→Settle

pretreatment appears to be optimal. On the other hand, it is difficult to remove denser

cakes by hydraulic or chemical cleaning. To provide practically useful guidelines on

the optimal choice of pretreatment a study of membrane cleaning efficiency as a

function of pretreatment conditions is necessary.

In direct filtration experiments, Low$\overline{G}t_{mix}$→Direct pretreatment conditions (-●-,

Figure 4-12) illustrated the smallest flux decline. The reason behind this smallest flux

decline was the relatively low fraction of feed solids (60.3%, Figure 4-8) that fouled

the membrane. Despite differences in the floc structure as a function of $\overline{G}t_{mix}$(D_{floc}^{CM} =

2.12 for Low$\overline{G}t_{mix}$ versus 2.72 and 2.67 for Med$\overline{G}t_{mix}$ and High$\overline{G}t_{mix}$), there was no

statistically significant difference in specific cake resistances. These results indicated

that flocs generated under Low$\overline{G}t_{mix}$→Direct conditions were prone to restructuring.

CONCLUSIONS AND RECOMMENDATIONS

5.1 CONCLUSIONS

Coagulation parameters such as coagulant dose, pH and mixing conditions (G and t) play important role on clay floc characteristics i.e., size and fractal dimensions. Two synthetic clay suspensions with different turbidity were used and coagulated under different coagulation conditions (Low and high$\overline{G}t_{mix}$) to see the effect of coagulation parameters. A comparison was also drawn between conventional filtration and direct filtration for all experimental conditions ($\overline{G}t_{mix}$ and turbidity difference). The conclusions drawn from the clay flocs study are:

1. Results revealed that flocs of higher fractal dimensions were achieved on high $\overline{G}t_{mix}$ conditions.

2. There was significant influence of clay floc characteristics on membrane fouling and specific cake resistance (α_m).

3. Pre-settling also has a direct effect on ultrafiltration. Porosity and resistance of membrane cake is dependent on floc size. Porosity of the membrane cake of clay increases with its thickness.

4. Results show the higher specific cake resistances (α_m) were achieved in case of low turbidity for both conventional and direct filtration conditions.

5. On the basis of these results it was concluded that direct filtration is only feasible for low turbidity water (10-15 NTU). In high turbidity water (30-35 NTU) direct filtration will enhance the load on membrane.

6. Scaling of the clay membrane cake was observed by using a non-invasive method. Different pretreatment conditions gave different scaling exponents. A high variation was observed in values of D_{floc} as compared to the values of D_{cake}.

Structural characteristics of humic acid flocs and membrane cakes were studied to interpret the effect of pretreatment and ultrafiltration on an aqueous solution of humic acid. Three flocculation regimes (low, medium and high $\bar{G}t_{mix}$) were studied with the option of pre-settling of flocculated suspension in one set of experiments before the ultrafiltration and without pre-settling in other set of experiments. The experimental plan was designed to roughly estimate the three pretreatment choices from inline (low $\bar{G}t_{mix}$, no pre-settling), to direct (medium or high $\bar{G}t_{mix}$, no pre-settling), to conventional filtration (medium or high $\bar{G}t_{mix}$, pre-settling). The results obtained from humic acid flocs study are:

1. Pretreatment has a strong effect on membrane permeate flux and specific cake resistance. Results obtained from the fractal dimension of humic acid flocs (D_{floc}, measured by light scattering and confocal microscopy) and the fractal dimension of membrane cake (D_{cake}) established a connection between pretreatments conditions and ultrafiltration performance.

2. For estimating D_{cake} a non-invasive method was proposed in this study and we found excellent scaling results. Different pretreatment conditions gave statistically different scaling exponents for each pretreatment condition.

3. For all experimental conditions cake porosity was calculated by using experimentally measured specific cake resistance data and semi-empirical permeability-porosity correlation (Happel equation). The results showed that the average cake porosity increased with the increase in permeate volume except very early stages of cake growth and that increase in cake porosity can be quantified in terms of the fractal dimension, D_{cake}. To our knowledge this study is first to report that a scaling law is applied to the growth of cake porosity.

4. Humic acid flocs of different sizes and fractal dimensions were produced as a result of different flocculation conditions, flocs of higher fractal dimensions were produced by high $\bar{G}t_{mix}$ conditions. The only effect of pre-settling was of increasing specific cake resistance by removing larger humic acid flocs from the membrane feed and had no effect on flocs with certain fractal dimension on the other hand.

5. A weak correlation (R^2=0.86) was established for values of D_{floc} and D_{cake} for humic acid flocs. A broad range of D_{floc} values from 1.95 to 2.56 (resultant to different pretreatment conditions) ended up into a narrow range of D_{cake} values

(from 2.92 to 2.99) representing the importance of humic acid flocs breakup and restructuring as they fitted into a growing cake.

6. A weak correlation between D_{floc} and D_{cake} translated that the liaison between floc and cake microstructure was not strong. However, the choice of flocculation regime (i.e. the choice of $\bar{G}t_{mix}$- the main determinant of D_{floc}) was applicable for permeate flux performance.

5.2 RECOMMENDATIONS

Whilst this study explored various combinations of suspension characteristics and mixing and treatment conditions as they affect floc characteristics, following research ideas can still be proposed for further development of this area and creation of new knowledge.

1. To study the influence of velocity gradient (G) variation, on alum and/or titanium tetrachloride floc characteristics i.e., size, strength, shape and fractal dimension and effect of floc characteristics on microfiltration and/or ultrafiltration membranes under a range of coagulation conditions (pH, temperature, coagulant dose, strength of synthetic water and G) and hydraulic loading rates.

2. The conclusions of this study can be tested in field conditions and natural water samples.

3. Dominant mechanisms of reversible and irreversible membrane fouling can be elucidated during ultrafiltration and microfiltration of pre-coagulated water

using one of blocking models (Combined pore-blockage-cake-filtration model, Carman-Kozeny model or Happel model.)

4. The effectiveness of treatment by the polymeric ultrafiltration and microfiltration membranes of a range of porosities can be compared.

Chapter 6

REFERENCES

Adachi, Y., S. Ooi, Geometrical structure of a floc, J. Colloid Interface Sci. 135 (1990) 374-384.

Antelmi, D., B. Cabane, M. Meireles, P. Aimar, Cake collapse in frontal filtration, Langmuir, 17 (2001) 7137-7144.

AWWA, 1997. Water treatment plant design. American Water Works Association, American Society of Civil Engineers, Third Edition, McGraw-Hill, New York.

Bache, D.H., E. Rasool, D. Moffat, F.J. McGilligan, On the strength and character of alumino-humic flocs, Water Sci. Technol. 40 (1999) 81–88.

Bouyer, D., C. Coufort, A. Line, Z. Do-Quang, Experimental analysis of the floc size distribution in a 1-L jar under different hydrodynamics and physicochemical conditions, J. Colloid Interface Sci. 292 (2005) 413–428.

Bowen, W. R., F. Jenner, Theoretical description of membrane filtration of colloids and free particles: an assessment and review, Adv. Colloidal Interface Sci. 56 (1995) 141-200.

Bushell, G.C., Y.D. Yan, D. Woodfield, J. Raper, R. Amal, On techniques for the measurement of the mass fractal dimension of aggregates, Adv. Colloidal Interface Sci. 95 (2002) 1-50.

Byun, S., J.S. Taurozzi, A.L. Alpatova, F. Wang, V.V. Tarabara, Performance of polymeric membranes treating ozonated surface water: Effect of ozone dosage, Separ. Puri. Technol. 81 (2011) 270-278.

Carroll, T., S. King, S.R. Gray, B.A. Bolto, N.A. Booker, The fouling of microfiltration membranes by NOM after coagulation treatment, Water Res. 34 (11) (2000) 2861-2868.

Chakraborti, R.K., J.F. Atkinson, J.E. Van Benschoten, Characterization of alum floc by image analysis, Environ. Sci. Technol. 34 (2000) 3969–3976.

Chakraborti, R.K., K.H. Gardenr, J.F. Atkinson, J.E. Van Benschoten, Changes in fractal dimension during aggregation, Water Res. 37 (2003) 873–883.

Chakraborti, R.K., K.H. Garder, J.F. Atkinson, J.E. Van Benschoten, Changes in fractal dimension during aggregation, Water Research 37 (2003) 873-883.

Cho, M.-H., C.-H. Lee, S. Lee, Influence of floc structure on membrane permeability in the coagulation-MF process, Water Sci. & Technol. 51 (2005) 143-150.

Cho, M.-H., C.-H. Lee, S. Lee, Influence of floc structure on membrane permeability in the coagulation-MF process, Water Sci. & Technol. 51 (2005) 143-150

Colomer, J., F. Petersb, C. Marrase, Experimental analysis of coagulation of particles under low-shear flow, Water Res. 39 (2005) 2994–3000.

Cornet, P., R. Summers, P. Roberts, Diffusion of humic acid in dilute aqueous solutions, J. Colloid Interface Sci. 110 (1) (1986) 149-160

Dennett, K.E., A. Amirtharajah, A. Studstill, T.F. Moran, J.P. Gould, Humic Substance Removal and Minimization of Trihalomethanes by Ferric Chloride Coagulation, AWWARF, Denver, Colorado, USA, 1995

Dulebohn, J., P. Ahmadiannamini, T. Wang, S.-S. Kim, T.J. Pinnavaia, V.V. Tarabara, Polymer mesocomposites: Ultrafiltration membrane materials with enhanced permeability, selectivity and fouling resistance, J. Membr. Sci., 453 (2014) 478-488.

Ghosh, K., M. Schnitzer, Macromolecular structures of humic substances, Soil Sci. 129 (1980) 266-278

Gregory, J,. The density of particle aggregates, Water Sci. Technol. 36 (1997) 1–13.

Harmant, P., P. Aimar, Coagulation of colloids in a boundary layer during crossflow filtration, Colloids Surf. A, 138 (1998) 217-230.

Huang, X., K. Xiao, Y. Shen, Recent advances in membrane bioreactor technology for wastewater treatment in China, Front. Environ. Sci. Eng. China 4 (2010) 245–271.

Jarvis, P., B. Jefferson, and S.A. Parsons, Breakage, regrowth, and fractal natural organic matter flocs. Environ. Sci. Technol., 2005. 39(7): p. 2307-2314.

Jarvis, P., B. Jefferson, J. Gregory, S.A. Parsons, A review of floc strength and breakage, Water Res. 39 (2005) 3121–3137.

Jarvis, P., B. Jefferson, S.A. Parsons, Breakage, regrowth, and fractal natural organic matter flocs., Environ. Sci. Technol., 39 (2005) 2307-2314.

Jiang, Q., B.E. Logan, Fractal dimensions of aggregates determined from steady-state size distributions, Environ. Sci. Technol. 25 (1991) 2031–2038.

Johnson, C.P., X.Y. Li, B.E. Logan, Settling velocities of fractal aggregates, Environ. Sci. Technol. 30 (1996) 1911–1918.

Khan, E., R.W. Babcock, I.H. Suffet, M.K. Stenstorm, Biodegradable dissolved organic carbon for indication plant performance and treated wastewater quality, Water Environ. Res. 70 (1998) 1033-1040

Koen, G., V. Willy, Image analysis to estimate the settleability and concentration of activated sludge, Water Res. 31 (1997) 1126–1134.

Koen, G., V. Willy, Image analysis to estimate the settleability and concentration of activated sludge, Water Research 31 (1997) 1126-1134.

Lai, R. J., H.E. Hudson, J.E. Singley, Velocity-gradient calibration of jar-test equipment, J. Am. Water Works Assn., 67 (1975) 553-557.

Le-Clech, P., V. Chen, T.A.G. Fane, Fouling in membrane bioreactors used in wastewater treatment, J. Membr. Sci. 284 (2006) 17–53.

Lee, D.G., J.S. Bonner, L.S. Garton, A.N.S. Ernest, R.L. Autenrieth, Modeling coagulation kinetics incorporating fractal theories: comparison with observed data, Water Research 36 (2002) 1056-1066

Lee, J.D., S.H. Lee, M.H. Jo, P.K. Park, C.H. Lee, J.W. Kwak, Effect of coagulation conditions on membrane filtration characteristics in coagulation-microfiltration process for water treatment, Environ. Sci. Technol. 34 (17) (2000) 3780-3788.

Lee, S.A., A.G. Fane, T.D. Waite, Impact of natural organic matter on floc size and structure effects in membrane filtration, Environ. Sci. Technol., 39 (2005) 6477-6486.

Letterman, R.D., A. Amirtharajah, Charles R. O'Melia, Chapter 6, Coagulation and Flocculation,1999.

Li, T., Z. Zhu, D. Wang, C. Yao, H. Tang, Characterization of floc size, strength and structure under various coagulation mechanisms, Powder Technol. 168 (2006) 104-110.

Li, X.-Y., B.E. Logan, Permeability of fractal aggregates, Water Res., 35 (2001) 3373-3380.

Logan, B.E., J.R. Kilps, Fractal dimensions of aggregates formed in different fluid mechanical environments, Water Res. 29 (2) (1995) 443-453.

MacFarlane, I.C., Muskeg Engineering Handbook, in, University of Toronto Press, 1969.

Mallevialle, J., Odendaal, P. E., and Wiesner, M. R., in "Water Treatment Membrane Processes" (J. Mallevialle, P. E. Odendaal, and M. R. Wiesner, Eds.) Chap. 1, pp. 1.1-1.10. McGraw-Hill, New York, 1996.).

Matilainen, M., Vepsäläinen, M. Sillanpää, Natural organic matter removal by coagulation during drinking water treatment: a review, Adv. Colloid Interface Sci. 159 (2010) 189–197.

McCurdy, K., K. Carlson, D. Gregory, Flocs morphology and cyclic shearing recovery: comparison of alum and polyaluminum chloride coagulants,Water Res. 38 (2004) 486–494.

Meeten, G.H., A dissection method for analysing filter cakes, Chem. Eng. Sci., 48 (1993) 2391-2398.

Mendret, J., C. Guigui, P. Schmitz, C. Cabassud, In situ dynamic characterisation of fouling under different pressure conditions during dead-end filtration: Compressibility properties of particle cakes, J. Membr. Sci., 333 (2009) 20-29.

Mendret, J., C. Guigui, P. Schmitz, C. Cabassud, P. Duru, An optical method for in situ characterisation of fouling during filtration, AIChE J., 53 (2007) 2265-2274.

Meng, F.G., S.R. Chae, A. Drews, M. Kraume, H.S. Shin, F.L. Yang, Recent advances in membrane bioreactors (MBRs): membrane fouling and membrane material, Water Res. 43 (2009) 1489–1512.

Metcalf and Eddy, Inc., 2003. Wastewater Engineering: Treatment, Disposal and Reuse, third ed., McGraw-Hill, Boston, MA.

Odriozola, G., Tirado-Miranda, M., Schmitt, A., Martinez López, F., Callejas-Fernández, J., Martínez-García, R. and Hidalgo-Álvarez, R., A Light Scattering Study of the Transition Region between Diffusion- and Reaction-Limited Cluster Aggregation, Journal of Colloid and interface Science 240, 90-96 (2001)

Oles, V., Shear-induced aggregation and breakup of polystyrene latex-particles, J. Colloid Interface Sci. 154 (2) (1992) 351–358.

Park, P.-K., C.-H. Lee, S. Lee, Permeability of collapsed cakes formed by deposition of fractal aggregates upon membrane filtration, Environ. Sci. Technol., 40 (2006) 2699-2705.

Rattanakawin, C., R. Hogg, Aggregate size distributions in flocculation, Colloids Surf. A: Physicochem. Eng. Aspects Sci. 177 (2001) 87–98.

Ripperger, S., W. Gosele, C. Alt, Filtration , in: Ullmann's Encyclopedia of Industrial Chemistry, Wiley-VCH, Weinheim, 2012, pp. 677-709.

Rojas, J.C., B. Moreno, G. Garralón, F. Plaza, J. Pérez, M.A. Gómez, Influence of velocity gradient in a hydraulic flocculator on NOM removal by aerated spiral-wound ultrafiltration membranes (ASWUF), J. Hazard. Mater. 178 (2010) 535–540.

Serra, T., J. Colomer, B.E. Logan, Efficiency of different shear devices on flocculation, Water Res. 42 (2008) 1113–1121.

Serra, T., J. Colomer, X. Casamitjana, Aggregation and breakup of particles in a shear flow, J. Colloid Interface Sci. 187 (2) (1997) 466–473.

Siddiqui, M.S., G.L.Amy, B.D. Murrhy, Ozone enhanced removal of natural organic matter from drinking water source, Water Research, 31(1997) 3098-3106).

Spicer, P.T., S.E. Pratsinis, J. Raper, R. Amal, G. Bushell, G. Meesters, Effect of shear schedule on particle size, density and structure during flocculation in stirred tanks, Powder Technol. 97 (1998) 26–34.

Spicer, P.T., S.E. Pratsinis, Shear-induced flocculation: the evolution of floc structure and the shape of the size distribution at steady state, Water Res. 30 (5) (1996) 1049–1056.

Spicer, P.T., Shear-induced aggregation-fragmentation: mixing and aggregate morphology effects, Doctor Dissertation, 1997.

Waite, T.D., S. Andreal, G.F. Anthony, H. Axel, Colloidal fouling of ultrafiltration membranes: Impact of aggregate structure and size. J. Colloid Interface Sci., 212 (1999) 264-274.

Tambo, N., H. Hozumi, Physical characteristics of flocs: strength of flocs, Water Res. 13 (1979) 421–427.

Tambo, N., Y. Watanabe, Physical characteristics of floc-: the floc density function and aluminium floc, Water Res. 13 (1978) 409–419.

Tan, B.H,. P. Ravi, L.N. Tan, K.C. Tam, Synthesis and aqueous solution properties of sterically stabilized pH-responsive polyampholyte microgels, J. Colloid Interface sci. 309 (2007) 453–463.

Tanaka, H., T. Araki, Simulation method of colloidal suspensions with hydrodynamic interactions: fluid particle dynamics, Phys. Rev. Lett. 85 (2000) 1338–1341.

Tang, P., J. Greenwood, J.A. Raper, A model to describe the settling behavior of fractal aggregates, J. Colloid Interface Sci. 247 (2002) 210–219.

Tang, P., J. Greenwood, J.A. Raper, A model to describe the settling behavior of fractal aggregates, Journal of Colloid and Interface Science 247 (2002) 210-219

Tarabara, V.V., I. Koyuncu, M.R. Wiesner, Effect of hydrodynamics and solution ionic strength on permeate flux in cross-flow filtration: direct experimental observation of filter cake cross-sections, J. Membr. Sci., 241 (2004) 65-78.

Terao, T., T. Nakayama, Sol–gel transition of reversible cluster–cluster aggregations, Phys. Rev. E 58 (1998) 3490–3494.

Thill, A., S. Veerapaneni, B. Simon, M. Wiesner, J.Y. Bottero, D. Snidaro, Determination of structure of aggregates by confocal scanning laser microscopy. J. Colloid Interface Sci., 204 (1998) 357-362.

Thill, A., et al., Determination of structure of aggregates by confocal scanning laser microscopy. J. Colloid Interface Sci., 1998. 204: p. 357-362

Thill, A., M. Wagner, J.Y. Bottero, Confocal scanning laser microscopy as a tool for the determination of 3D floc structure, J. Colloid Interface Sci. 220 (1999) 465–467.

Veerapaneni, S., M.R. Wiesner, Hydrodynamics of fractal aggregates with radially varying permeability, J. Colloid Interface Sci., 177 (1996) 45-57.

Waite, T.D., A.I. Schafer, A.G. Fane, A. Heuer, Colloidal fouling of ultrafiltration membranes: Impact of aggregate structure and size, J. Colloid Interface Sci., 212 (1999) 264-274.

Waite, T.D., et al., Colloidal fouling of ultrafiltration membranes: Impact of aggregate structure and size. J. Colloid Interface Sci., 1999. 212: p. 264-274.

Waite, T.D., Measurement and implications of floc structure in water and wastewater treatment, Colloids and Surfaces A, 151(1999) 27-41

Waite, T.D., Measurement and implications of floc structure in water and wastewater treatment, Colloid Surface A, 151 (1999) 27-41.

Wang, D., R. Wu, Y. Jiang, C.W.K. Chow, Characterization of floc structure and strength: Role of changing shear rates under various coagulation mechanism, Colloids and Surfaces A: Physicochem. Eng. Aspects 379 (2011) 36-42.

Wang, J., J. Guan, S. R. Santiwong, T. D. Waite, Effect of aggregate characteristics under different coagulation mechanisms on microfiltration membrane fouling, Desalination 258 (2010) 19-17.

Wang, J., J. Guan, S.R. Santiwong, T. D. Waite, Characterization of floc size and structure under different monomer and polymer coagulants on microfiltration membrane fouling, J. Membr. Sci. 321 (2) (2008) 132-138.

Wang, J., J. Guan, S.R. Santiwong, T.D. Waite, Effect of aggregate characteristics under different coagulation mechanisms on microfiltration membrane fouling, Desalination, 258 (2010) 19-27.

Wang, Y.G., C. Combe, M.M. Clark, The effects of pH and calcium on the diffusion coefficient of humic acid, J. Membr. Sci., 183 (2001) 49-60.

Weisner, M. R., and Aptel, P., in "Water Treatment Membrane Processes" (J. Mallevialle, P. E. Odendaal, and M. R. Wiesner, Eds.) Chap.4, pp. 4.1-4.30. McGraw-Hill, new York, 1996

Witten, T.A., L.M. Sander, Diffusion-limited aggregation: a kinetic critical phenomenon, Phys. Rev. Lett. 47 (1981) 1400–1403.

Wu, R.M., D.J. Lee, T.D. Waite, J. Guan, Multilevel structure of sludge flocs, J. Colloid Interface Sci. 252 (2002) 383–392.

Wu, R.M., D.J. Lee, T.D. Waite, J. Guan, Multilevel structure of sludge flocs, Journal of Colloid and Interface Science 252 (2002) 383-392.

Xiao, F., J. H. Huang, B. Zhang and C. Cui, Effect of low temperature on coagulation kinetics and floc surface morphology using alum, Desalination 237(2009) 201-213

Xiao, F., X.R. Pan, P. Yi, B.J. Zhang, C. Lee, Comparative study of the effects of experimental variables on growth rates of aluminum and iron hydroxide flocs

during coagulation and their structural characteristics, Desalination 250 (2010) 902–907.

Yu, W., G. Li, Y. Xu, X. Yang, Breakage and re-growth of flocs formed by alum and PACl, Powder Technol. 189 (2009) 439-443.

Yukselen, M.A., J. Gregory, The reversibility of floc breakage, Intl. J. Miner. Proces. 73 (2004) 251–259.

Zhan, X., B. Gao, Y. Wang, Q. Yue, Influence of velocity gradient on aluminum and iron floc property for NOM removal from low organic matter surfacewater by coagulation, Chem. Eng. J. 166 (2011) 116-121.

Zularisam, A.W., A.F. Ismail, R. Salim, Behaviours of natural organic matter in membrane filtration for surface water treatment—a review, Desalination 194 (2006) 211–231.

DEFINITIONS

Coagulation	The chemical process of destabilization of colloidal matter. Double layer compression, adsorption-charge neutralization, inter-particle bridging, and sweep coagulation are the four well known destabilization mechanisms.
Coagulant	Chemicals that are added to raw water to destabilize the suspended particles. Examples of coagulants are aluminum sulfate, ferric sulfate, and variety of organic polymers.
Turbidity	The light scattering property of a suspension. Units are nephelometric turbidity units (NTU).
Flocculation	The slow mixing of coagulated water to aggregate the destabilized particles and form a floc.
G	The velocity gradient (sec^{-1})
T	Residence time in the rapid mix basin (sec)
Optimum Dose	The coagulant dose that gives the minimum filter effluent turbidity measured after equilibrium is established. Filter effluent turbidity declines with time until the coagulants has full effect (at about 10 min after the start of the experiment), (mg/L)
Floc Characteristics	Physico-chemical properties of the coagulated particles such as mean diameter, particle size distribution, shape, density, and shear strength
Mean Diameter	Measurement of length in a particular direction across the particle.
Density of Floc	Mass of solids per unit volume; relates to the settling capacity of floc in a medium (mg/ml)
Floc Strength	Resistance to fragmentation by shear forces induced by hydraulic velocity gradients.
Zeta Potential	A measure of rate of movement of particles in the electrical field at a specified temperature (mV).
Uniformity	It is equal to the sieve size passing 60 percent of the sand divided

Coefficient (UC)	by that size passing 10 percent.
Transport Step	First step in filtration that involves the transport of suspended particles to the filter grains.
Attachment Step	The second step in filtration involving chemical forces making the suspended particle to attach to the filter grain.
Turbidity wavefront	A turbidity-depth curve for a given time
Filter coefficient	The constant of proportionality for the Iwasaki's (1937) relationship between the rate of change of residual turbidity and the depth of the filter bed.
Breakthrough	The point at which the filtrate turbidity starts increasing with time.
Fractal dimension of floc	A fractal dimension is an index for characterizing fractal patterns or sets by quantifying their complexity as a ratio of the change in detail to the change in scale.
Diffusion-limited aggregation	Diffusion-limited aggregation is the process whereby particles undergoing a random walk due to Brownian motion cluster together to form aggregates of such particles.
Reaction-limited aggregation	When the interaction potential shows an intermediate barrier, the aggregation is slowed down by the fact that numerous attempts will be necessary to overcome this barrier, and one refers to slow or reaction limited aggregation (RLA)
Reynolds number	The Reynolds number is defined as the ratio of inertial forces to viscous forces and consequently quantifies the relative importance of these two types of forces for given flow conditions.
Pre-settling	Pre-Settling is the process by which particulates settle to the bottom of a liquid and form a sediment.
Stokes-Einstein equation	In the limit of low Reynolds number, the mobility μ is the inverse of the drag coefficient ζ. A damping constant $\gamma = \zeta/m$ is frequently used for the momentum relaxation time (time needed for the inertia momentum to become negligible compared to the random momenta) of the diffusive object. For spherical particles of radius r, Stokes' law gives:

$$\zeta = 6\pi\eta r,$$

where η is the viscosity of the medium. Thus the Einstein-Smoluchowski relation results into the Stokes-Einstein relation

$$D = \frac{k_B T}{6\pi\eta r}$$

In the case of Rotational diffusion, the friction is $\zeta_r = 8\pi\eta r^3$, and the rotational diffusion constant D_r is

$$D_r = \frac{k_B T}{8\pi\eta r^3}$$

Ultrafiltration	Ultrafiltration (UF) is a variety of membrane filtration in which forces like pressure or concentration gradients leads to a separation through a semipermeable membrane.
Permeate flux	A membrane's flux is defined as flow divided by the membrane area.
Membrane resistance (R_m)	The membrane resistance is a measure of the impediment to the transmembrane flow through the membrane.
Cake porosity	A measurement of the open space in a membrane cake. Also called open area or voids volume.
Dynamic light scattering	Dynamic light scattering is a technique in physics that can be used to determine the size distribution profile of small particles in suspension or polymers in solution.
Intra-aggregate porosity	Porosity between two aggregates
Inter-aggregate porosity	Porosity within one aggregate
Carman-Kozeny equation	The Carman-Kozeny–equation is a relation used in the field of fluid dynamics to calculate the pressure drop of a fluid flowing through a packed bed of solids.

Cake thickness	The height of foulants deposit on the surface of the membrane in the form of cake is called cake thickness.
Membrane fouling	Membrane fouling is a process where solute or particles deposit onto a membrane surface or into membrane pores in a way that degrades the membrane's performance.
Pearson product moment correlation coefficient	In statistics, the Pearson product-moment correlation coefficient is a measure of the linear correlation (dependence) between two variables X and Y, giving a value between +1 and −1 inclusive, where 1 is total positive correlation, 0 is no correlation, and −1 is total negative correlation.
Membrane cake permeability	Membrane cake permeability refers to the ability of water to pass through the membrane cake.
Flocs break-up	In the process of flocculation the already prepared flocs tend to break up because of the shear applied in flocculation.
Flux decline	When a new membrane is first placed in service, the flux tends to be high. Over the next hour or two, the flux falls off dramatically. This fall in flux with time is called flux decline.
Model feed water matrix	Model water prepared to study the effect of velocity gradient in this study.
Inline filtration	In inline filtration the coagulant is added in coagulation basin having contaminated water to be treated. Only rapid mixing is provided and no flocculation and settling provided in this system. Flocs will form as the water having coagulant moves in the water supply pipes.
Direct filtration	In direct filtration coagulation and flocculation is done to treat water and settling is not provided prior to filtration.
Conventional filtration	In conventional filtration all three steps of water treatment i.e. coagulation, flocculation and sedimentation or settling is provided prior to filtration.

PUBLICATIONS AND CONFERENCE PRESENTATIONS

1. Amjad, H., Z., Khan, V.V. Tarabara, Fractal structure and permeability of membrane cake layers: Effect of 4 coagulation–flocculation and settling as pretreatment steps, Sep. Purif. Technol. 143 (2015) 40-51.

2. Amjad, H., Z., Khan, A comparison of Fractal Dimensions of Clay and Humic Acid Flocs under Optimum Coagulation Conditions, Presented at the **6th International Conference on Environmental Engineering and Applications**, Chengdu, China July 8-10, 2015.

3. Amjad, H., Z., Khan, A comparison of Fractal Dimensions of Clay and Humic Acid Flocs under Optimum Coagulation Conditions, **International Journal of Environmental Science and Development**, 7 (4) (2015) 240-243